OAK RIDGE
NATIONAL LABORATORY
MANAGED BY UT-BATTELLE
FOR THE DEPARTMENT OF ENERGY

ORNL/TM-2003/106

Assessment of Degree of Applicability of Benchmarks for Gadolinium Using KENO V.a and the 238-Group SCALE Cross-Section Library

December 2003

Prepared by

Sedat Goluoglu
C. M. Hopper

UT-BATTELLE
ORNL-27 (4-00)

ORNL/TM-2003/106

Nuclear Science and Technology Division (94)

Assessment of Degree of Applicability of Benchmarks for Gadolinium Using KENO V.a and the 238-Group SCALE Cross-Section Library

Sedat Goluoglu and C. M. Hopper

(865) 574-5255 (865) 576-8617
goluoglus@ornl.gov hoppercm@ornl.gov

Date Published: December 2003

Prepared by
OAK RIDGE NATIONAL LABORATORY
P.O. Box 2008
Oak Ridge, Tennessee 37831-6170
managed by
UT-BATTELLE, LLC
for the
U.S. DEPARTMENT OF ENERGY
under contract DE-AC05-00OR22725

CONTENTS

Page

LIST OF FIGURES

LIST OF TABLES

ACKNOWLEDGMENTS

This report provides the results of nuclear criticality safety (NCS) computational studies that were performed under subcontract for the U.S. Department of Energy (DOE) Environmental Management (EM) Office of Safety and Engineering specifically related to the NCS of waste disposition at the Savannah River Site. The collaboration among EM, DOE Environment, Safety and Health (EH), and DOE Contractor Site personnel identified an EM programmatic need and the NCS computational methods for addressing the need. The work was accomplished using the sensitivity and uncertainty methods tools that are under development at the Oak Ridge National Laboratory (ORNL). These tools are being made available through the continuing support of the DOE Nuclear Criticality Safety Program, which is managed by the National Nuclear Security Administration (NA) for the infrastructural benefit of the Department.

We express our appreciation to the personnel in these organizations for their recognition of the value of these tools for safely addressing operational needs within EM. Specifically, we appreciate the support of Ms. Sandra Johnson (EM) for enlisting the assistance of Dr. Jerry McKamy (EH) to identify EM's programmatic NCS needs and for her directing the fiscal support to ORNL to conduct pertinent studies demonstrating the value of the methods for economically addressing the NCS of EM operations. Also, we acknowledge Mr. Fitz Trumble of the Westinghouse Safety Management Solutions for identifying a specific operational NCS need to address the economic impact of waste disposition in glass logs. Appreciation is also extended to Dr. David Crandall (NA) and Mr. Michael Thompson (NA) for their active support for the development of a valuable infrastructural tool for NCS. Finally, appreciation is expressed to C. V. Parks, K. R. Elam, L. M. Petrie, Jr., and J. C. Wagner for their thorough reviews and comments. The careful formatting of this document by W. C. Carter and the editorial comments of M. K. Savage are also appreciated.

ABSTRACT

A review of the degree of applicability of benchmarks containing gadolinium using the computer code KENO V.a and the gadolinium cross sections from the 238-group SCALE cross-section library has been performed for a system that contains ^{239}Pu, H_2O, and Gd_2O_3. The system (practical problem) is a water-reflected spherical mixture that represents a dry-out condition on the bottom of a sludge receipt and adjustment tank around steam coils. Due to variability of the mixture volume and the $H/^{239}Pu$ ratio, approximations to the practical problem, referred to as applications, have been made to envelop possible ranges of mixture volumes and $H/^{239}Pu$ ratios. A newly developed methodology has been applied to determine the degree of applicability of benchmarks as well as the penalty that should be added to the safety margin due to insufficient benchmarks.

1. INTRODUCTION

Savannah River Site (SRS) has been processing plutonium into glass logs for long-term storage and/or disposal. Currently, iron, with its absorption properties, is being used during processing to provide criticality control. However, due to its relatively low neutron absorption [compared with gadolinium (Gd)], much greater quantities of iron relative to Gd are required for adequate criticality control. This scenario results in greater volumes of glass waste and therefore greater numbers of glass logs. Because of the potential benefit of using Gd instead of iron, the applicability of existing critical experiment benchmarks containing Gd relative to the possible validation of computational analyses for their intended use of Gd as a criticality control has been investigated.

Gadolinium is one of the strongest thermal neutron absorbers that can be used in nuclear criticality safety applications. Its very large absorption cross section has a strong effect on the spectrum of the system as it removes the thermal neutrons and hardens the neutron spectrum. As required by the American National Standards Institute, American Nuclear Society – 8.1-1998 standard, "Nuclear criticality safety in operations with fissionable material outside reactors," the calculational method used for a process safety analysis must be validated to ensure that the method and data are applicable to the analysis. In that regard, it is necessary to verify and validate the Gd cross-section data that are used for safety calculations. The validation requires benchmarks that are neutronically similar to the application that is considered in the process safety analysis in order to establish a computational bias and uncertainty. Unfortunately, benchmarks with Gd are limited in number and generally do not match well with the application system due to differences between the neutronic properties of the benchmarks and the applications of interest. In this study, some benchmark experiments that are applicable to the SRS process have been identified. A new methodology has been developed to assess a computational penalty, which can be viewed as an additional margin of subcriticality, resulting from the application not being fully validated by the benchmarks. No computational bias or uncertainty has been determined, because actual validation of the code and the cross sections is beyond the scope of this study.

2. PROBLEM DESCRIPTION

A review of the degree of applicability of benchmarks containing Gd has been performed for a series of systems that contain ^{239}Pu, H_2O, and Gd_2O_3. The sensitivity of the effective multiplication factor (k_{eff}) for each system to each nuclide (for all reactions and all neutron energy groups) has been calculated with the SCALE (**S**tandardized **C**omputer **A**nalyses for **L**icensing **E**valuation) sensitivity/uncertainty (S/U) analysis tool TSUNAMI-3D,[1] which utilizes the Monte Carlo computer code KENO V.a. The integral parameters, which give a measure of the similarity between a given application and an experimental benchmark, are calculated with TSUNAMI-IP[2,3] code within SCALE using the sensitivity data. The Gd cross sections from the 238-group SCALE cross-section library have been used in the analysis. For applications that are not completely validated by available benchmarks, a new methodology has been developed for assigning a computational penalty based on the unvalidated data.

The application system is a water-reflected spherical mixture that represents a dry-out condition on the bottom of a sludge receipt and adjustment tank around steam coils. The mixture is modeled as a sphere in the middle of this water-filled cylindrical tank, which is 276 cm in diameter and 358 cm high. The fissile mass was specified as 4600 g ^{239}Pu (fixed amount determined by the operations). Due to variability of the mixture volume and H/^{239}Pu ratio, approximations, referred to as applications, have been modeled to envelop possible ranges of mixture volumes and H/^{239}Pu ratios. Thus, several application configurations were created to determine the effects of the sphere volume, the H/^{239}Pu ratio, and the amount of Gd present in the mixture. All application configurations have fixed plutonium masses of 4600 g ^{239}Pu but varying H/^{239}Pu and Gd/^{239}Pu ratios and several different sphere volumes. Since the application models are hypothetical configurations, some are nonphysical (e.g., more material than physically possible in a given volume) and some are very unlikely (e.g., very low density plutonium, water, and Gd_2O_3 mixture). As the volume of each application changes, the ^{239}Pu density also changes due to the fixed ^{239}Pu amount. The application with a H/^{239}Pu ratio of 1000 in a 225-L sphere with a Gd/^{239}Pu ratio of 1.0 (by weight) is referred to as the practical problem. Although the mixture in the practical problem is expected to have a Gd/^{239}Pu ratio of 1.0 (by weight), the amount of Gd present in the remainder of the application configurations has been varied to examine the influence of Gd concentration on k_{eff} and benchmark-to-application similarities. Note that the temperature effects have been neglected (i.e., room temperature has been assumed for all applications).

2.1 ANALYSES

A set of benchmark experiments has been selected for use in this study based on Gd content. Although some of the benchmarks within a series do not contain any Gd, these were not excluded from the set. Inclusion or exclusion of the benchmarks without any Gd has no effect on the analysis results. The benchmarks that have been selected are listed in Appendix A. Except for three in the "heust.018" series and one in the "puslgd" series, all of the benchmarks contain Gd. Unfortunately, a very limited number of critical experiments containing plutonium and Gd have been evaluated and included in the latest release of the International Handbook of Evaluated Criticality Safety Benchmark Experiments[4] (IHECSBE). The critical experiments that have been identified but are not in the handbook have been modeled using the best information available to the authors regarding these experiments.

The analyses have been performed for several sphere volumes, H/^{239}Pu ratios, and Gd amounts, as listed in Table 1. The minimum volumes for the ^{239}Pu mass (4600 g) and maximum water density have been determined to be 173.8, 124.8, and 87 L for H/^{239}Pu ratios of 1000, 718, and 500, respectively. The cases with a 150-L sphere and a H/^{239}Pu ratio of 1000 are nonphysical because they exceed the theoretical densities of the materials. This fact is indicated by actual-to-theoretical mixture density ratios of greater than 1.0, as listed in Table 1. The calculated k_{eff} values for all applications are listed in Table 1 and plotted in Fig. 1,

except for the practical problem case, which has a very small k_{eff} value (0.2434). The standard deviations were less than 0.0024 for all cases. The last case in Table 1 corresponds to the practical problem in terms of Gd density. This case demonstrates the effectiveness of Gd as a neutron absorber in quantities specified for the practical problem. It also shows how small the corresponding k_{eff} is expected to be for the practical problem.

As expected, when the Gd concentration increases, the system k_{eff} decreases. A plot of Gd concentrations in the applications and the benchmarks is given in Fig. 2. The case number locations in the figure (x-axis) are arbitrary and correspond to the values given in Table 1 for the applications and the values in Table A.1 in Appendix A for the benchmarks. Note that only the Gd concentrations for the first four applications and the practical problem are shown in the figure, because the rest of the application cases repeat the same (first four) sequence of Gd densities. The benchmarks that do not have any Gd are not shown in this figure (see Table A.2). For a given H/^{239}Pu ratio, the amount of ^{239}Pu and H_2O is fixed. Therefore, as the volume of the sphere increases, the ^{239}Pu and water density decrease and a homogeneous void fraction throughout the spherical material model is produced.

For each sphere volume and H/^{239}Pu ratio, four different Gd densities have been analyzed. These densities have been selected so that the calculated system k_{eff} values are ~1.0 (from 0.82 to 1.23). Since the Gd density rather than the total Gd in a sphere is varied, two spheres with different volumes but the same H/^{239}Pu ratios and Gd densities will contain different masses of Gd, with the larger volume containing the larger mass. When there is no Gd in the system, increasing the volume of the sphere (from 150 to 225 L) results in approximately 10% decrease in the calculated k_{eff} value for the same H/^{239}Pu ratio. With maximum-density Gd in the spheres, the difference in k_{eff} for the same systems is approximately 20%. Hence, additional Gd in the larger sphere is worth about 10% of the k_{eff} over the smallest sphere with the same H/^{239}Pu ratio. As the H/^{239}Pu ratio decreases, the k_{eff} also decreases, indicating that the systems are undermoderated. This decrease is illustrated in Fig. 3 for all application cases with 0.193 g/L Gd.

Table 1. Values of k_{eff} for all applications with fixed 4600-g ^{239}Pu mass

Case number	Sphere volume (L)	H/^{239}Pu	Gd (g/L)	Gd/^{239}Pu	k_{eff}	Ratio of actual to theoretical mixture density
1	150	1000	0.116	0.006	1.2314	1.16
2	150	1000	0.155	0.008	1.1888	1.16
3	150	1000	0.193	0.010	1.1485	1.16
4	150	1000	0.232	0.012	1.1147	1.16
5	150	718	0.116	0.006	1.2008	0.83
6	150	718	0.155	0.008	1.1575	0.83
7	150	718	0.193	0.010	1.1226	0.83
8	150	718	0.232	0.012	1.0887	0.83
9	150	500	0.116	0.006	1.1027	0.58
10	150	500	0.155	0.008	1.0693	0.58
11	150	500	0.193	0.010	1.0318	0.58
12	150	500	0.232	0.012	1.0048	0.58
13	175	1000	0.116	0.007	1.1749	0.99
14	175	1000	0.155	0.009	1.1380	0.99
15	175	1000	0.193	0.011	1.0936	0.99
16	175	1000	0.232	0.013	1.0554	0.99
17	175	718	0.116	0.007	1.1381	0.71
18	175	718	0.155	0.009	1.0956	0.71
19	175	718	0.193	0.011	1.0555	0.71
20	175	718	0.232	0.013	1.0228	0.71
21	175	500	0.116	0.007	1.0373	0.50
22	175	500	0.155	0.009	1.0004	0.50
23	175	500	0.193	0.011	0.9626	0.50
24	175	500	0.232	0.013	0.9348	0.50
25	200	1000	0.116	0.008	1.1333	0.87
26	200	1000	0.155	0.010	1.0869	0.87
27	200	1000	0.193	0.013	1.0450	0.87
28	200	1000	0.232	0.015	1.0045	0.87
29	200	718	0.116	0.008	1.0854	0.63
30	200	718	0.155	0.010	1.0380	0.63
31	200	718	0.193	0.013	0.9962	0.63
32	200	718	0.232	0.015	0.9620	0.63
33	200	500	0.116	0.008	0.9810	0.44
34	200	500	0.155	0.010	0.9359	0.44
35	200	500	0.193	0.013	0.9064	0.44
36	200	500	0.232	0.015	0.8701	0.44
37	225	1000	0.116	0.009	1.0948	0.77
38	225	1000	0.155	0.012	1.0412	0.77
39	225	1000	0.193	0.014	0.9971	0.77
40	225	1000	0.232	0.017	0.9537	0.77
41	225	718	0.116	0.009	1.0356	0.56
42	225	718	0.155	0.012	0.9872	0.56
43	225	718	0.193	0.014	0.9439	0.56

Table 1 (continued)

Case number	Sphere volume (L)	H/^{239}Pu	Gd (g/L)	Gd/^{239}Pu	k_{eff}	Ratio of actual to theoretical mixture density
44	225	718	0.232	0.017	0.9081	0.56
45	225	500	0.116	0.009	0.9250	0.39
46	225	500	0.155	0.012	0.8825	0.39
47	225	500	0.193	0.014	0.8451	0.39
48	225	500	0.232	0.017	0.8221	0.39
Practical problem	225	1000	20.445	1.520	0.2434	0.78

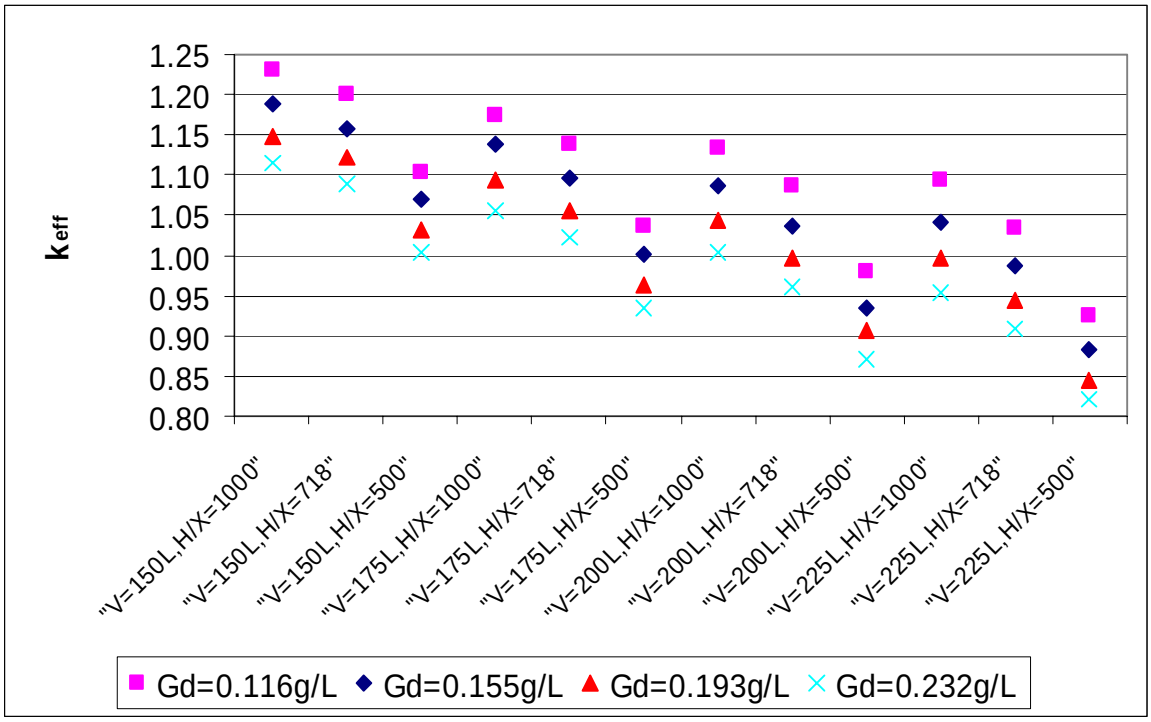

Fig. 1. Values of k_{eff} for the applications considered.

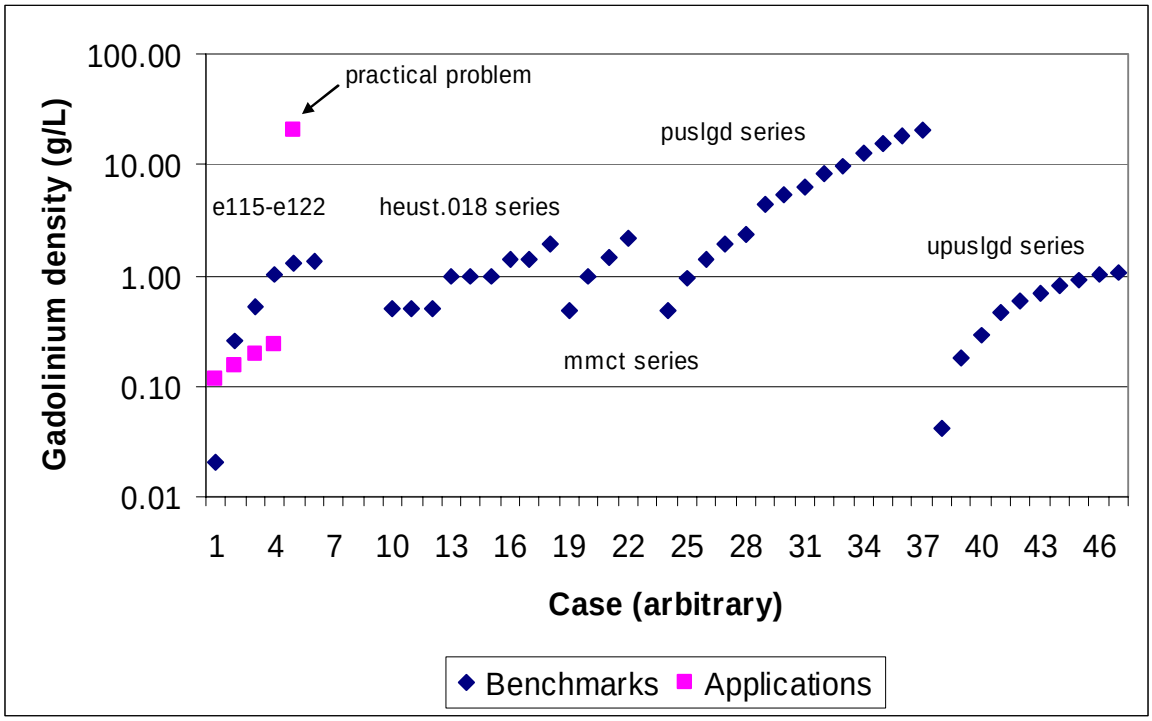

Fig. 2. Density of Gd in the applications and the benchmarks.

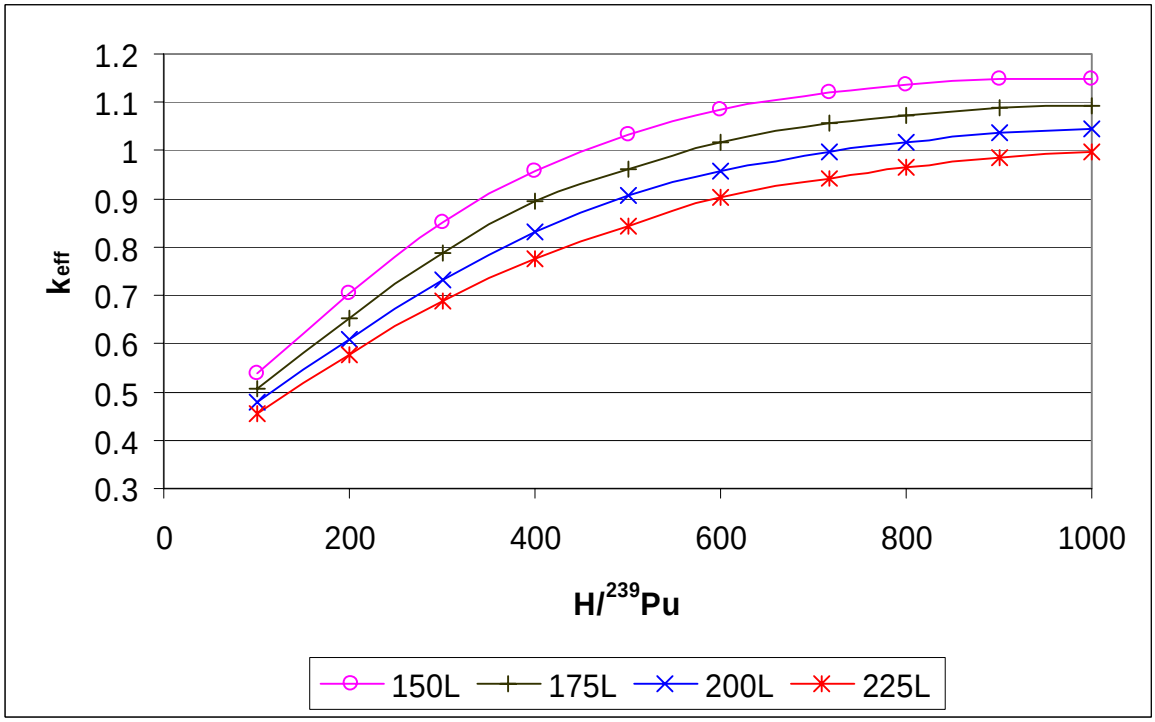

Fig. 3. Values of k_{eff} vs H/^{239}Pu for all applications with 0.193 g/L Gd.

3. METHODOLOGY

The analysis of the above applications has been performed using the S/U analysis tools, TSUNAMI,[1-3] which have been developed at Oak Ridge National Laboratory (ORNL). These S/U tools are based on first-order perturbation theory, in which the relative changes in the k_{eff} due to relative changes in the cross sections for each nuclide, reaction, and neutron energy group are calculated. Each nuclide, reaction (i.e., neutron capture, scattering, fission, etc., as well as the parameters $\bar{\nu}$ and χ), and energy group is referred to as a "triplet." A pair, on the other hand, is defined to be a specific nuclide and reaction (e.g., ^{157}Gd capture, ^{235}U fission). The triplets for a specific nuclide and reaction are summed over energy to obtain a pair. The relative change, or sensitivity, quantifies the importance of a nuclide–reaction–energy group triplet to the computed k_{eff} and, as such, is indicative of how important it is to know the reaction cross sections accurately. The main issue that is addressed in the remainder of this study is how to assess the computational penalty for an application with a significant number of triplets that are not covered by any combination of the benchmarks. Coverage is defined as having one or more benchmarks with sensitivities greater than the application's sensitivity for a specific nuclide–reaction–energy group triplet.

Using TSUNAMI, sensitivity profiles can be generated for each material in the system and may include various nuclear reactions (e.g., scatter, absorption, fission) as well as the neutron energy distribution from fission, χ, and the average number of neutrons emitted per fission, $\bar{\nu}$. The mathematical definition of a sensitivity "profile" is

$$S^{j,x,i} = \frac{\partial k_{eff} / k_{eff}}{\partial \Sigma^{j,x,i} / \Sigma^{j,x,i}}, \qquad \textbf{(1)}$$

where i is the neutron energy group index and x represents the reaction type (i.e., fission, scatter, capture, etc.) for nuclide j. The sensitivity coefficients (group value or sum over all groups) can be interpreted as percent change in the system k_{eff} for a 1% change in the cross section (corresponding group value or sum over all groups) for the reaction of interest.

The sensitivity of the system k_{eff} to each nuclide (for all reactions and all energy groups) is calculated with the TSUNAMI-1D[1] (formerly SEN1) or TSUNAMI-3D (formerly SEN3) sensitivity analysis tools for the application and all benchmarks for which similarity to the application is to be assessed. If any of the benchmarks exhibits greater sensitivities to the nuclide–reaction–energy group triplets than the application, then the benchmarks are considered to be appropriate for code and data validation for the application for those triplets. Consequently, the associated computational bias and uncertainty can be determined with some degree of confidence using an appropriate trending analysis. The determination of the degree of confidence in the computational bias and uncertainty is beyond the scope of this study and will be addressed by further research. In many cases, due to the limited number of benchmarks and diverse variety of application systems, many benchmarks would have to be combined to achieve complete coverage for all triplets. Some benchmarks may provide coverage for high-energy groups, while others may provide coverage for low-energy groups. If all triplets for an application are covered by the selected benchmarks, then the application is considered covered by the benchmarks that are included in the analysis and no computational penalty is assessed.

3.1 Integral Parameter *g*

The sensitivity differences for an application's triplet are computed by taking the group value for the application and subtracting the group value for each benchmark. This calculation produces a vector of values, each element of which represents the sensitivity difference between the application and the corresponding benchmark:

$$Z_{ab}^{j,x,i} = \begin{cases} S_a^{j,x,i} - S_b^{j,x,i}, & if \ \left|S_a^{j,x,i}\right| > \left|S_b^{j,x,i}\right| \ and \ S_a^{j,x,i} \cdot S_b^{j,x,i} > 0 \\ 0, & if \ \left|S_a^{j,x,i}\right| \le \left|S_b^{j,x,i}\right| \\ 0, & if \ S_a^{j,x,i} \cdot S_b^{j,x,i} < 0 \end{cases}, \quad \textbf{(2)}$$

where

i = the neutron energy group index;
j = the nuclide index;
x = the reaction index (e.g., fission, capture, etc.);
a = the application;
b = the benchmark;
$S_a^{j,x,i}$ = the application's sensitivity for neutron energy group i, nuclide j, and reaction x;
$S_b^{j,x,i}$ = the benchmark's sensitivity for neutron energy group i, nuclide j, and reaction x, and where the difference is taken only when the application's sensitivity triplet $S_a^{j,x,i}$ and the benchmark's sensitivity triplet $S_b^{j,x,i}$ have the same sign.

For each application triplet, there are as many sensitivity difference ($Z_{ab}^{j,x,i}$) values as there are benchmarks (i.e., b spans all benchmarks). The minimum of the sensitivity differences or the minimum noncoverage for the application is then the minimum of the $Z_{ab}^{j,x,i}$ values for each triplet calculated over all benchmarks:

$$Z_a^{j,x,i} = \min(Z_{ab}^{j,x,i}), \quad \textbf{(3)}$$

where b spans all benchmarks.

The sum of the minimum sensitivity differences over all energy groups ($Z_a^{j,x}$) is defined as the minimum of the sensitivity differences:

$$Z_a^{j,x} = \sum_i Z_a^{j,x,i} \ . \quad \textbf{(4)}$$

Coverage for a nuclide-reaction pair is assessed by analyzing the normalized differences in sensitivities between the application and each benchmark. This normalized difference for each nuclide and all reactions of interest is defined as

$$g'_{j,x} = \frac{\sum_i Z_{ab}^{j,x,i}}{\sum_i S_a^{j,x,i}}, \quad \textbf{(5)}$$

where the difference ($Z_{ab}^{j,x,i}$) is calculated based on the conditional Eq. (2).

A g' value is calculated for an application against each benchmark for each nuclide-reaction pair. Hence, for *N* benchmarks there are *N* g' values for an application for each nuclide-reaction pair. For a specific nuclide-reaction pair, the integral parameter g' is defined as the summed difference between the sensitivity coefficients for an application and a benchmark for all energy groups where the application's sensitivity is greater than the benchmark's sensitivity, normalized with respect to the application's total sensitivity. Total sensitivity is defined as the sensitivity for a specific nuclide-reaction pair that results from summation of the sensitivity triplets over all energy groups. Hence, throughout this document, total sensitivity should not be understood as representing the sensitivity of the total cross section.

The normalization of g' bounds its values between 0 and 1. A g' value of 0 indicates complete coverage (i.e., $\left|S_a^{j,x,i}\right| < \left|S_b^{j,x,i}\right|$ for all triplets), whereas a g' value of 1 indicates a complete noncoverage due to the benchmark's sensitivity being exactly zero. A large g' value indicates that the application's sensitivity for a specific nuclide-reaction pair is greater than the benchmark's sensitivity for the same nuclide-reaction pair in some or all neutron energy groups. Moreover, a large g' value indicates that the summed difference $Z_{ab}^{j,x}$ is a large fraction of the application's sensitivity.

Consider a hypothetical application that has high sensitivity only in the low-neutron-energy range (i.e., high below 1 eV and zero above 1 eV) for an arbitrary nuclide-reaction pair. Also consider a hypothetical benchmark that has high sensitivity only in neutron energies above 1 eV for the same nuclide-reaction pair (i.e., high above 1 eV and zero below 1 eV). The g' value for this case would be exactly 1. If the application's sensitivity above 1 eV is nonzero, then the g' value would be less than 1 and the actual value would depend on how large the application's sensitivity is in this range (i.e., above 1 eV). Similarly, if the benchmark's sensitivity below 1 eV is nonzero, then the g' value would be less than 1 and the actual value would depend on how large the benchmark's sensitivity is in this range (i.e., below 1 eV).

Historically, the integral parameters that have been used in the sensitivity analysis have been defined such that a normalized integral parameter value of 1 indicates total agreement. Therefore, a slightly different version of the integral parameter g', which can be thought of as the complement parameter, has been defined as follows:

$$g_{j,x} = 1 - g'_{j,x} = 1 - \frac{\sum_i Z_{ab}^{j,x,i}}{\sum_i S_a^{j,x,i}}, \quad \textbf{(6)}$$

where a g value of 1 indicates complete coverage and a g value of 0 indicates a complete noncoverage due to benchmark's sensitivity being exactly zero.

In Fig. 4, the mathematical interpretation of the *g* value is illustrated as differences between the application and benchmark sensitivities. In the energy range where the application's sensitivity is greater than the benchmark's sensitivity, the difference is calculated and is shown as the shaded area in the figure. The energy

range of the shaded area indicates that for which the application's sensitivities are not covered by the benchmark. The g' value is the ratio of this shaded area, $\sum_i Z_{ab}^{j,x,i}$, to the area under the application's sensitivity curve, $\sum_i S_a^{j,x,i}$. Then, the g value is simply $(1-g')$. By definition, covered triplets do not contribute to the numerator of g'. Thus, the degree of coverage for a specific triplet does not influence the value of g. This feature is advantageous over previous nuclide-reaction-specific integral parameters, which could be artificially inflated by triplets where the benchmark's sensitivity greatly exceeds that of the application.

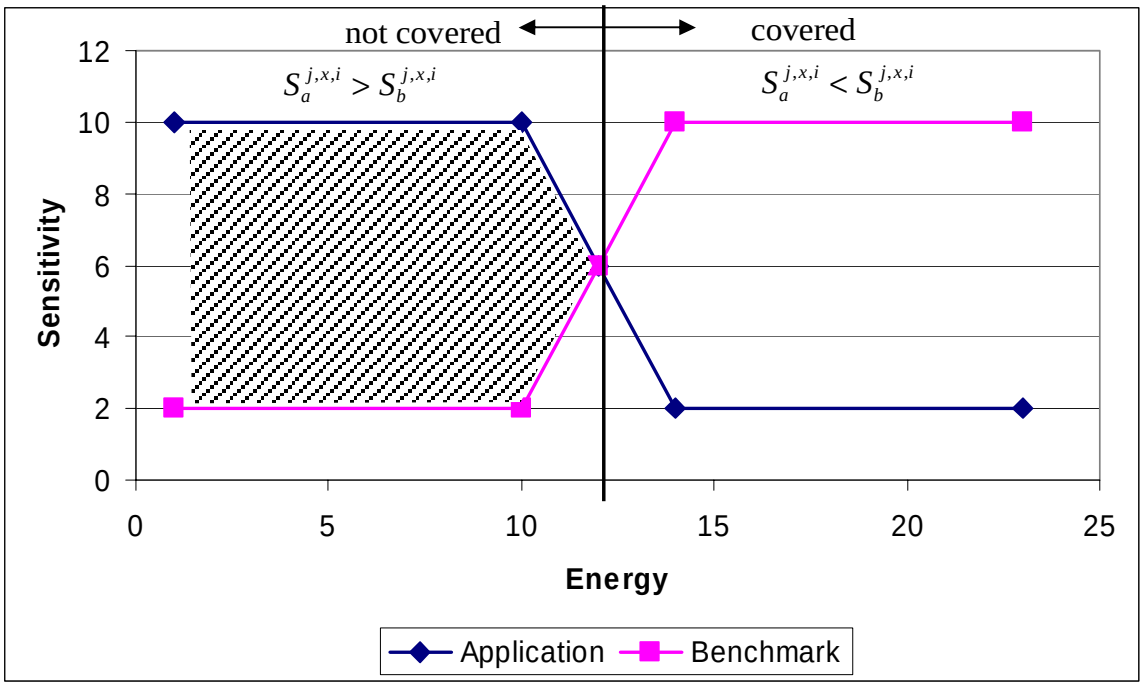

Fig. 4. Illustration of *g* value.

A large g value indicates that the covered part of the application's sensitivity for a specific nuclide-reaction pair makes up the majority of the application's sensitivity for that pair. Though not necessary to consider in the analysis, if the value of the total sensitivity for a nuclide-reaction pair is "small," the application can be considered adequately covered by the benchmark over all energy groups for that nuclide-reaction pair, even with a small g value. Here "small sensitivity" is arbitrarily defined as resulting in less than 0.001 change in k_{eff} for a 100% change in the cross sections. If an application is completely covered, there is no need to determine a computational penalty due to noncoverage.

The differences between the application and benchmark sensitivities are indicative of how well the benchmark covers the application. If these differences are small, then the benchmarks are considered adequate for the application for validation purposes and the effect of the uncertainties in the cross-section data would be quantified by trending analysis. If the differences are large, then the benchmarks are not adequate for the application for validation and the computational penalty that is generated is not appropriate. The sensitivity difference value above which these differences are considered large has not been established in this study.

That task is beyond the scope of this study and will be concluded in the future as part of the development of a guidance document on the use of the *g* parameter methodology for assessment of the degree of applicability of benchmarks and the corresponding computational penalty due to noncoverage.

3.2 Estimated Penalty

The penalty assessment methodology presented here is based on the assumption that a benchmark with a greater sensitivity for the nuclide, reaction and energy group triplet of interest sufficiently covers the triplet in the application. The approach that is used in this method is to determine the differences between the application and benchmark sensitivities for all triplets that are not covered and to quantify the importance of this noncoverage in terms of its final effect on the k_{eff} value of the application using the cross-section uncertainties.

In the penalty assessment, the application's sensitivity for a nuclide-reaction pair is compared against all benchmarks that are included in the analysis on a group-wise basis. All nuclide-reaction pairs are processed sequentially (one at a time). For each pair being processed, the number of benchmarks that have greater sensitivities than the application is tallied for each group for adequacy of coverage. If some of the groups have no benchmarks that provide coverage, then the minimum of the sensitivity differences (noncoverage) between all benchmarks and the application for those noncovered groups is calculated (i.e., shaded area in Fig. 4).

Before a sensitivity difference between the application and a benchmark can be used in the penalty assessment, the application and each considered benchmark must pass the similarity test based either on the integral parameter c_k or the integral parameter E_{sum}. These parameters are described in detail in Ref. 2. In this study, the integral parameter c_k, which is defined as the correlation coefficient between the uncertainties in two systems, has been used to establish the similarity between two systems, namely the application and the benchmark. The c_k parameter has been chosen because it utilizes the cross-section covariance data to assess the similarity between an application and a benchmark. Hence, the sensitivity differences for the benchmarks that do not pass the similarity test between the benchmark and the application are eliminated from the vector. Determining the similarity of benchmarks to the application by using the integral parameter c_k results in a corresponding bias and uncertainty, which is incorporated into the subcritical limit. The method by which this bias is determined is beyond the scope of this study.

The minimum of the sensitivity differences can be viewed as a measure of the inadequacy of the benchmark suite to replicate the physics of the application. This minimum sensitivity difference can be converted into an artificial computational penalty by multiplying the difference by the cross-section covariance data for that nuclide-reaction pair. If the covariance data for the desired nuclide-reaction pair do not exist, a hypothetical matrix corresponding to 10, 20, 100%, etc., uncertainty in the cross-section data can be used to quantify possible effects from the nuclide-reaction pair, assuming linearity of k_{eff} response to cross section. One should keep in mind, however, that first-order linear perturbation theory is valid for small changes in the variable (i.e., in this case, the uncertainty that is propagated to the final result). As such, it would be appropriate to choose a hypothetical matrix value that bounds the expected maximum uncertainty effect on the penalty. This approach, though not theoretically appropriate, is very useful for examining and estimating cross-section impacts on the computed results. If the analyst has *a priori* knowledge regarding the cross-section uncertainties (at least the magnitude), a corresponding conservative matrix value can be selected. For example, if the uncertainties are not known but are expected to be less than 20%, then the penalty value from 20% or larger uncertainty value can be used in determining the penalty. In this study, a 100% uncertainty in the cross sections for which there are no covariance data has been assumed.

The cross-section uncertainties and the minimum sensitivity differences are used to calculate an adjusted k_{eff}, which is interpreted to be the application's calculated k_{eff}, increased for consideration of noncovered sensitivities. The adjusted k_{eff} (k'_{eff}) is the k_{eff} value after accounting for the noncoverage:

$$k'_{eff} = k_{eff} + k_{eff}\sqrt{Z_a C_{\alpha\alpha} Z_a^{\,T}} \; . \qquad \textbf{(7)}$$

For N triplets in the problem, Z_a is an $N \times 1$ vector of the minimum of the sensitivity differences comprised of $Z_a^{j,x,i}$ values for all nuclides, reactions, and energy groups; $Z_a^{\,T}$ is the transpose; and $C_{\alpha\alpha}$ is the $N \times N$ cross-section covariance matrix. Hence, N is the number of nuclide-reaction pairs times the number of neutron energy groups (i.e., the number of triplets). In the above equation, the unit for Z_a is $(\Delta k_{eff} / k_{eff}) / (\Delta\Sigma / \Sigma)$ and the unit for $C_{\alpha\alpha}$ is $(\Delta\Sigma / \Sigma)^2$. Therefore, the final penalty has the unit (Δk_{eff}). The cross-section uncertainty is $(\Delta\Sigma / \Sigma)$ [e.g., 10% uncertainty in the cross sections implies that $(\Delta\Sigma / \Sigma)$ is 0.1].

Hence, the adjusted k_{eff} represents the calculated effective multiplication factor after applying a penalty for the noncoverage of the sensitivities. The noncoverage is weighted by the uncertainties in the measured cross sections, thereby creating a penalty that is the result of the cross-section uncertainties. If the cross-section uncertainties were zero (implies cross sections are known exactly), then the penalty would be zero, even if the application's sensitivities were not covered completely. This result is reasonable and expected, because if the cross sections are known exactly, there would not be any concern about validating the cross sections or determining the degree of applicability of the benchmarks based on the cross sections. Therefore, no penalty would have to be assessed due to cross-section uncertainties.

Currently, a single benchmark can provide coverage for an application. The adequacy of coverage by one benchmark has not yet been investigated. An alternate use of the g value may be developed in the future to increase the adjusted k_{eff} penalty when an insufficient number of benchmarks (e.g., one) provide coverage.

4. APPLICATION TO ^{157}Gd CAPTURE

The energy-integrated ^{157}Gd capture sensitivities for the applications and the benchmarks that have been used in this study are shown in Figs. 5 and 6, respectively. The case numbers in Fig. 6 correspond to the benchmark case numbers in Table A.1. Note that the benchmarks with no Gd have ^{157}Gd capture cross-section sensitivity values of zero. Among all Gd isotopes, ^{157}Gd has been selected for detailed analysis due to its large capture cross-section sensitivity compared with other Gd isotopes for the applications that have been analyzed in this study. The ^{157}Gd and ^{155}Gd capture cross-section sensitivities of a representative application are shown in Fig. 7. Only ^{155}Gd and ^{157}Gd are shown in this figure, since the capture cross-section sensitivities for all other Gd isotopes are more than two orders of magnitude smaller across the entire neutron energy range. The value "a" in the legend indicates the total sensitivity for the reaction that is being plotted. If the sensitivity profile has a mixture of positive and negative sensitivity values, then the values that are opposite in sign to the total sensitivity ("a=") are shown with "osc=" in the legend.

The spheres with the largest volume (i.e., 225 L) have been selected for further detailed analysis. Among the 225-L spheres, the application configuration with 0.232 g/L Gd and a H/^{239}Pu ratio of 1000 has the largest sensitivity to the ^{157}Gd capture cross section. Therefore, the application case for the 225-L sphere with 0.232 g/L Gd and a H/^{239}Pu ratio of 1000 will be used for the remainder of this study to demonstrate the application of the assessment methodology to determine the penalty due to insufficient coverage by the available benchmarks. In the remainder of this report, the word "application" will denote this selected application configuration.

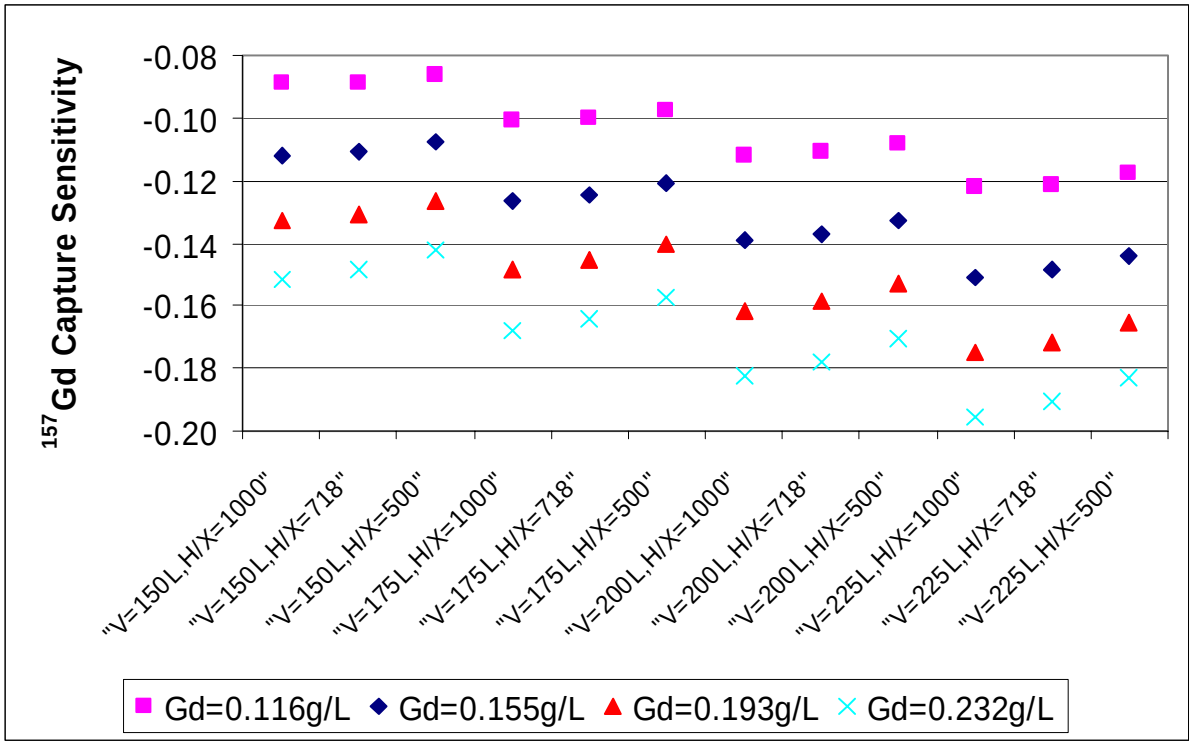

Fig. 5. Energy-integrated ^{157}Gd capture sensitivities for applications.

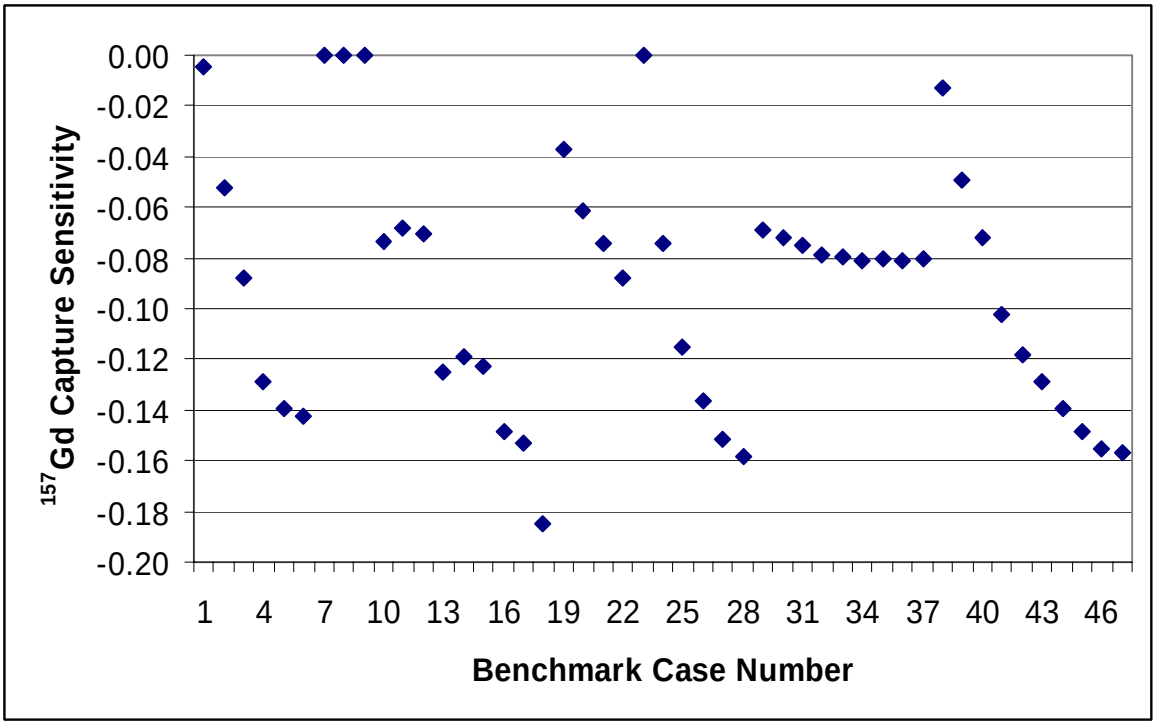

Fig. 6. Energy-integrated ^{157}Gd capture sensitivities for benchmarks.

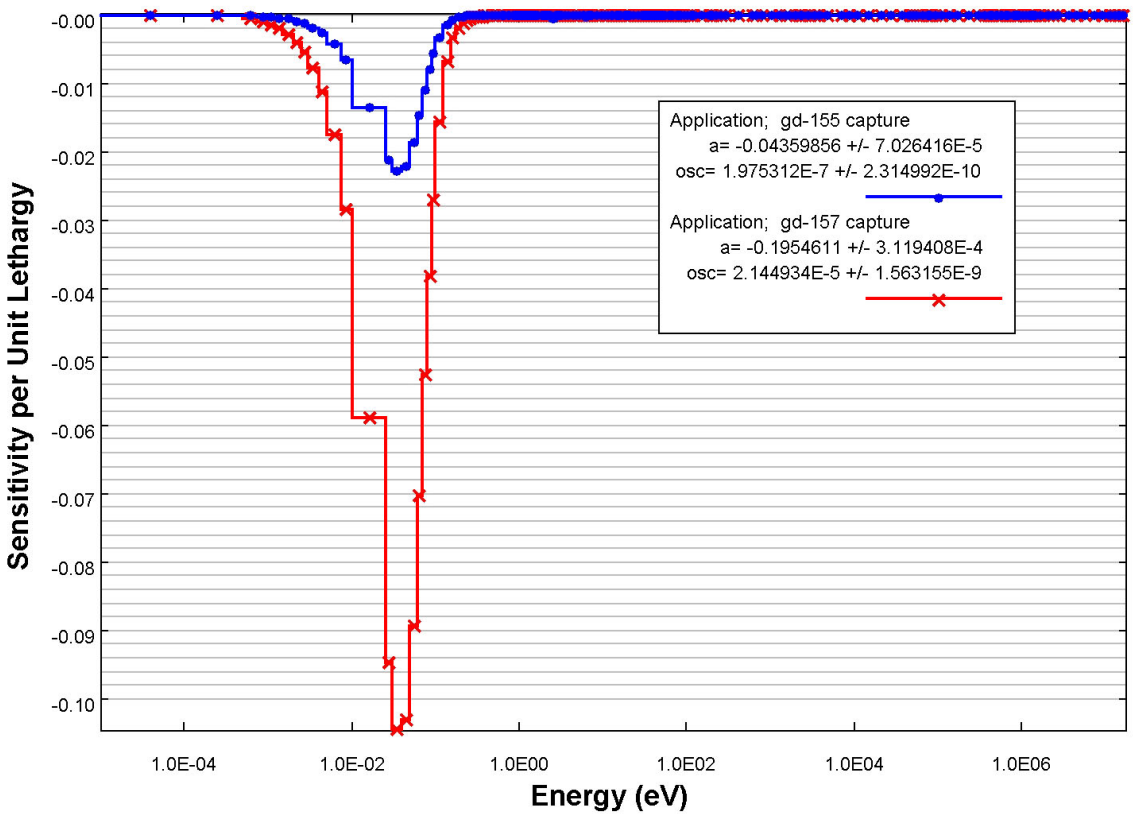

Fig. 7. Capture sensitivity for ^{155}Gd and ^{157}Gd isotopes.

The system characteristics and calculated parameters for the specific application of interest are listed in Table 2. The application's sensitivity to the ^{157}Gd capture is shown in Fig. 8, along with the capture cross section. The ^{157}Gd capture sensitivity profile for the application is plotted in Fig. 9, along with the sensitivity profiles of the benchmarks that yield the largest *g* value for ^{157}Gd capture from each benchmark series. Note that the sensitivities above 1 eV are on the order of 10^{-5} or less and therefore are indistinguishable in the figure.

Table 2. System characteristics and ^{157}Gd capture sensitivities for 225-L sphere with H/^{239}Pu of 1000

Characteristic/Parameter	Value
H/^{239}Pu	1000
Gd density (g/L)	0.232
Percent flux < 0.625 eV	41.23
Percent flux = 0.625 eV–100 keV	25.87
Percent flux > 100 keV	32.90
^{157}Gd capture sensitivity	–0.19546 ± 3.1194E–4
Value of *g* for ^{157}Gd capture	0.8093
Benchmark that yields largest *g* for ^{157}Gd capture	heust.018-case_12
^{157}Gd capture sensitivity for the benchmark that yields largest *g* for ^{157}Gd capture	–0.18512 ± 2.6953E–4

Analysis of ^{157}Gd capture cross-section sensitivities from all benchmarks that were used in this study indicates that the benchmark designated with name "heust.018-case12" exhibits the largest sensitivity. The ^{157}Gd capture cross-section sensitivities from this benchmark and the application are shown in Fig. 10. For sensitivity plots with log y-axis scale, the negative sensitivities have been inverted in sign before plotting because negative values cannot be plotted on a logarithmic scale. This procedure is indicated in the legend of the plot by using different line styles for negative and positive values and labeling these lines accordingly.

The application's ^{157}Gd capture cross-section sensitivity is greater than that of the benchmark in the thermal energy range (below ~0.05 eV). The ^{157}Gd capture cross-section sensitivities in this range are the greatest, which result in a *g* value of ~0.81, indicating that the covered part of the application's ^{157}Gd capture cross-section sensitivity makes up approximately 81% of the application's total ^{157}Gd capture cross-section sensitivity.

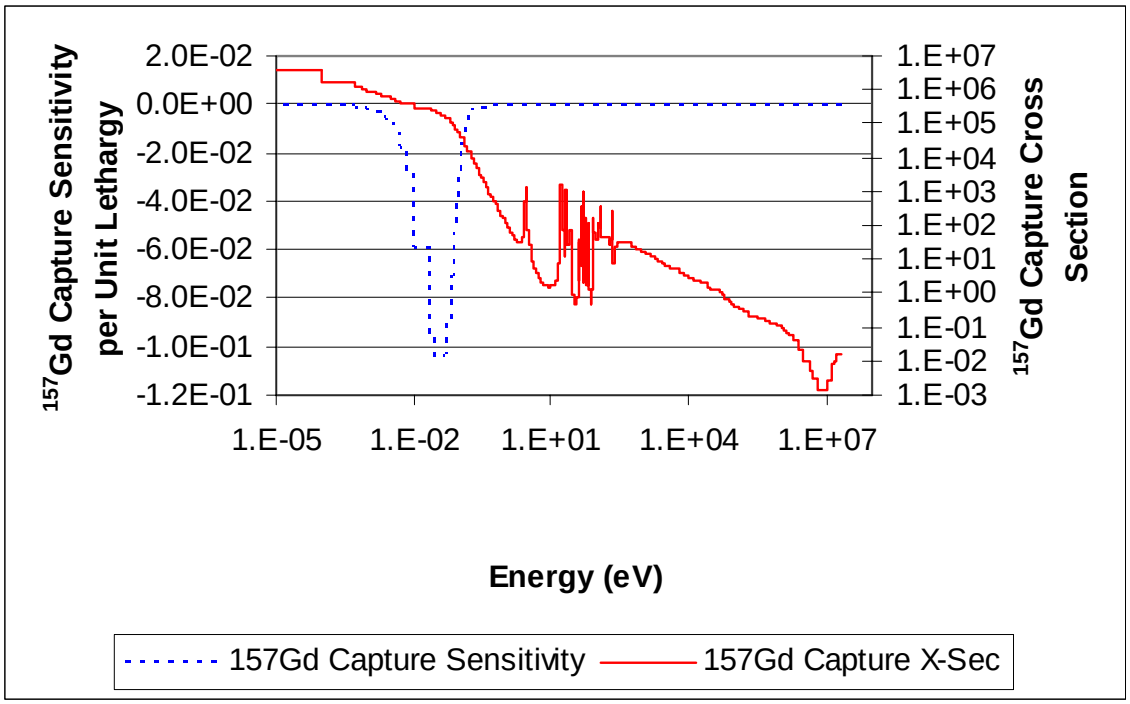

Fig. 8. Capture cross section and sensitivity for ^{157}Gd.

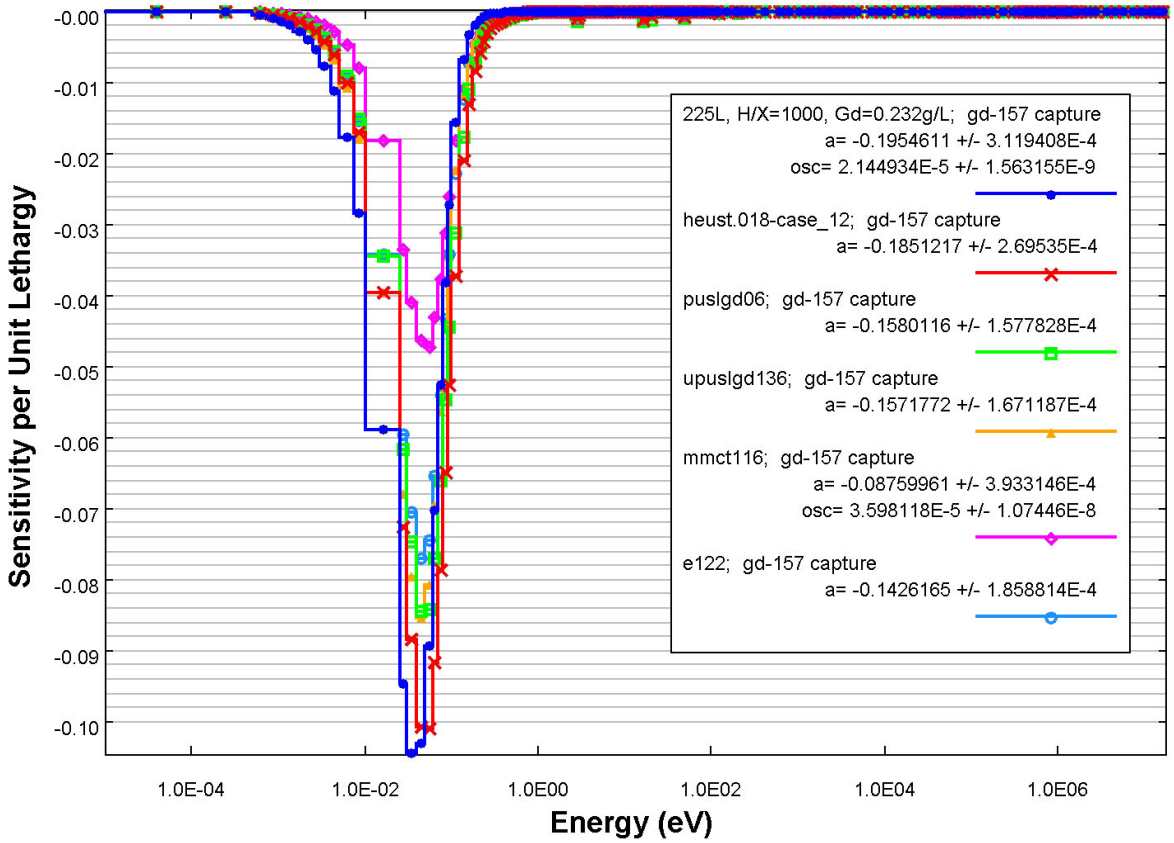

Fig. 9. Capture cross-section sensitivity profiles for ^{157}Gd.

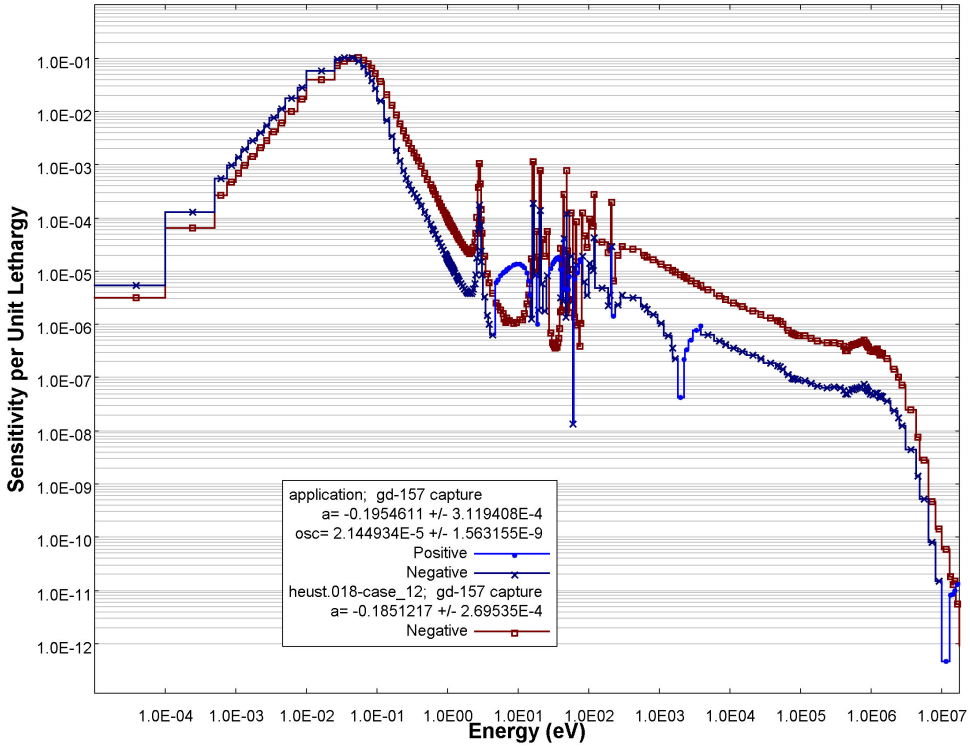

(a) full energy spectrum

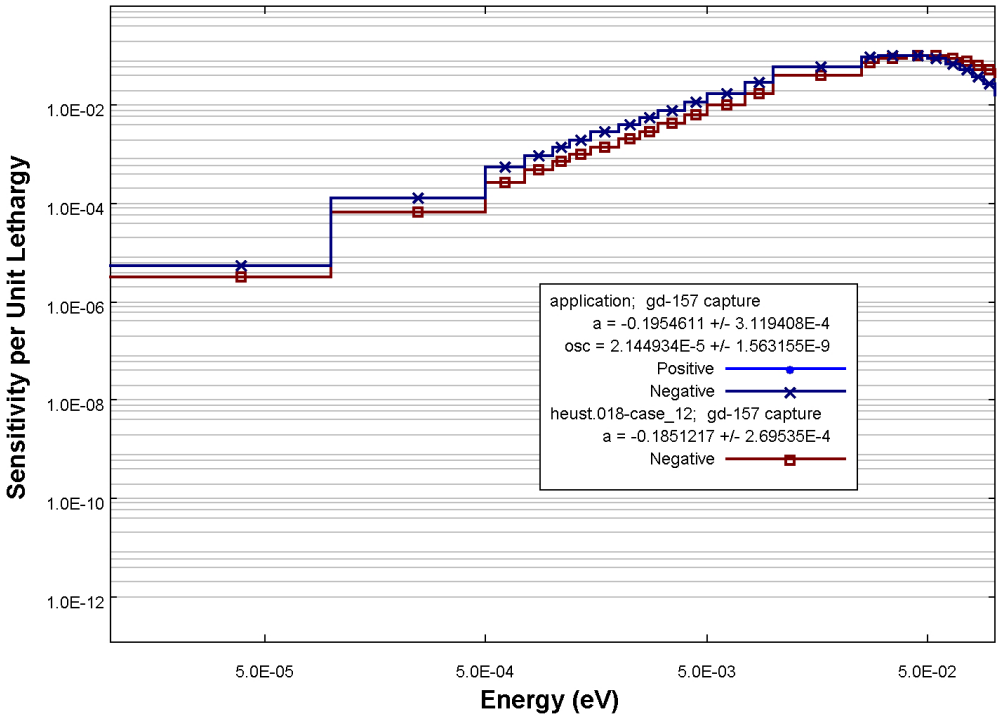

(b) energy range for which $S_a > S_b$

Fig. 10. Comparison of heust.018-case12 and the application.

The values for neutron energy of average lethargy causing fission (EALF) for all benchmarks and the application are shown in Fig. 11. The case number locations in the figure (x-axis) are arbitrary and correspond to the values given in Table A.1 in Appendix A for the benchmarks. The EALF value for the application is less than half the EALF values for the benchmarks, which indicates that the neutrons in the application system are more thermalized than the benchmarks. Therefore, despite having Gd concentrations that are lower than those in the real application, the application system is more sensitive to the ^{157}Gd capture cross sections, which are larger in the thermal energy range, as shown in Fig. 8.

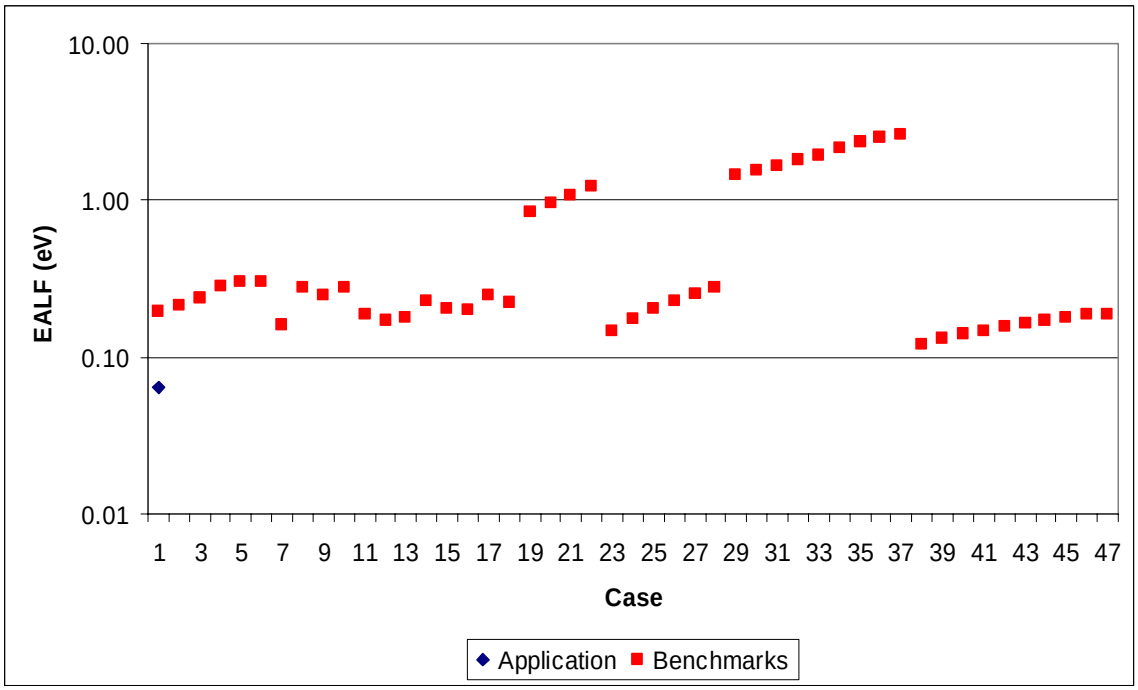

Fig. 11. Energy of average lethargy causing fission (arbitrary case numbers).

When the maximum *g* value is less than 1.0, which implies that less than 100% of the application's sensitivity is covered by any benchmark, the sum of differences for the groups that are not covered (noncoverage) is used to determine the importance of this noncoverage. The minimum of sensitivity differences ($Z_a^{j,x,i}$, where *j* is the nuclide ^{157}Gd, *x* is the capture reaction, and *i* is the neutron energy group) in ^{157}Gd capture sensitivities between the application and the benchmarks that provide the closest sensitivity for the groups that are not covered is shown in Fig. 12 and designated as "composite."

A composite profile is one that is created by comparing, on a group-wise basis, the sensitivity value of an application with all benchmarks and selecting the sensitivity value of the benchmark that is closest to the application's value. If there exist some benchmarks that have larger sensitivity values than the application, then the sensitivity value of the composite profile is set equal to that of the application. Mathematically, the composite profile can be expressed as $S_{composite}^{j,x,i} = S_a^{j,x,i} - Z_a^{j,x,i}$, where $Z_a^{j,x,i}$ is the minimum difference in the group-wise sensitivity coefficient for nuclide *j*, reaction *x*, and neutron energy group *i* and where $S_a^{j,x,i}$ is the application's sensitivity. Note that the benchmark that provides the closest sensitivity may be different for each group.

As shown in Fig. 12, the application is almost completely covered above approximately 0.05 eV. Furthermore, the composite and application profiles coincide, except for minor differences in the resolved resonance range and very high neutron energies. Below 0.05 eV, there is no coverage, which is evidenced by the composite profile that shows smaller group sensitivities for ^{157}Gd capture. The sum of the minimum sensitivity differences for the groups that are not covered ($Z_a^{j,x}$) is approximately –0.0361. The total sensitivity for ^{157}Gd capture for this application is –0.1955. Thus, the noncovered portion of the application's sensitivity represents ~18% of the sensitivity.

The number of benchmarks that provide coverage for the ^{157}Gd capture sensitivity of the application as a function of neutron energy group is plotted in Fig. 13. Above neutron energy group 221 (neutron energy 0.05 eV and below), there is no coverage by any of the benchmarks (as Fig. 12b also indicates). Because the ^{157}Gd capture sensitivity of the application is greatest below 0.05 eV, this noncoverage is the main contributor to a small *g* value and a large sum of the minimum sensitivity differences [$Z_a^{j,x}$ for nuclide *j* (i.e., ^{157}Gd) and reaction *x* (i.e., capture)].

Since the noncoverage is calculated after evaluating the coverage by benchmarks collectively, the noncoverage is generally smaller than the *g* value might suggest. The difference between the application and the benchmark (heust.018-case_12), for which the application's sensitivity to ^{157}Gd capture is greater than that of the benchmark, is –0.0361. The sum of the differences is folded with the cross-section covariance data to compute the penalty to be applied to the calculated k_{eff} value. Assuming 100% uncertainty in the cross sections for which there are no covariance data in the cross-section library, the penalty for the application is calculated to be 2.91% ($\Delta k_{eff}/k_{eff}$). Therefore, the adjusted k_{eff} value for the application, which is interpreted to be the application's calculated k_{eff} increased for consideration of noncovered sensitivities, is 0.9814; that is

$$k'_{eff} = k_{eff} + k_{eff}\sqrt{Z_a C_{\alpha\alpha} Z_a^{\ T}},$$

$$k'_{eff} = 0.9537 + 0.9537 * 0.0291,$$

and

$$k'_{eff} = 0.9814.$$

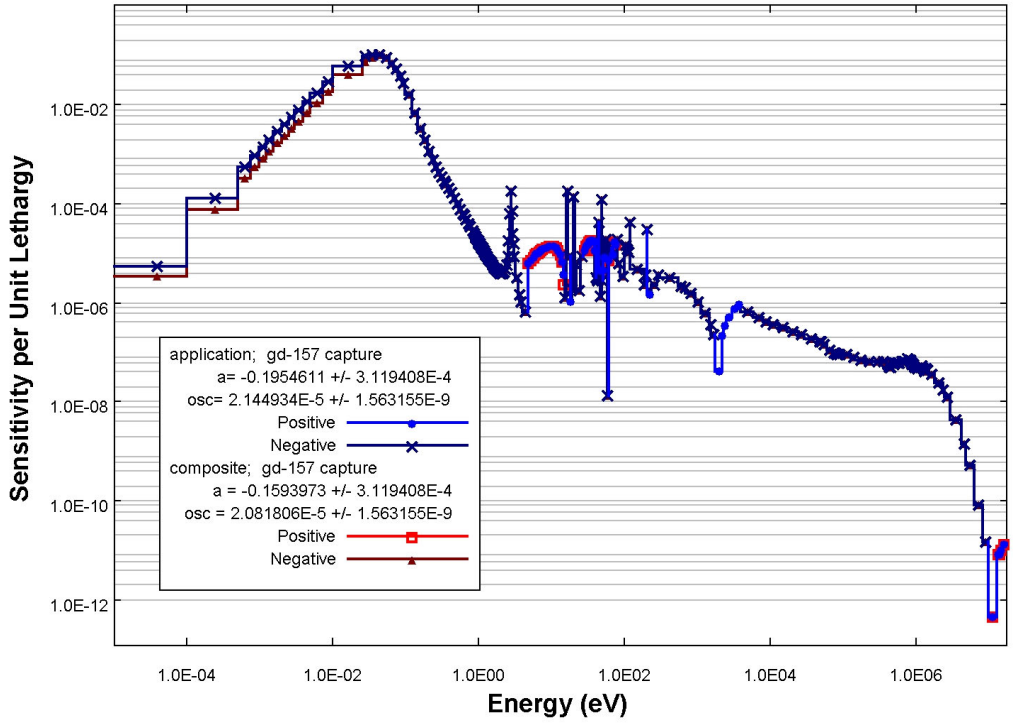

(a) full energy range

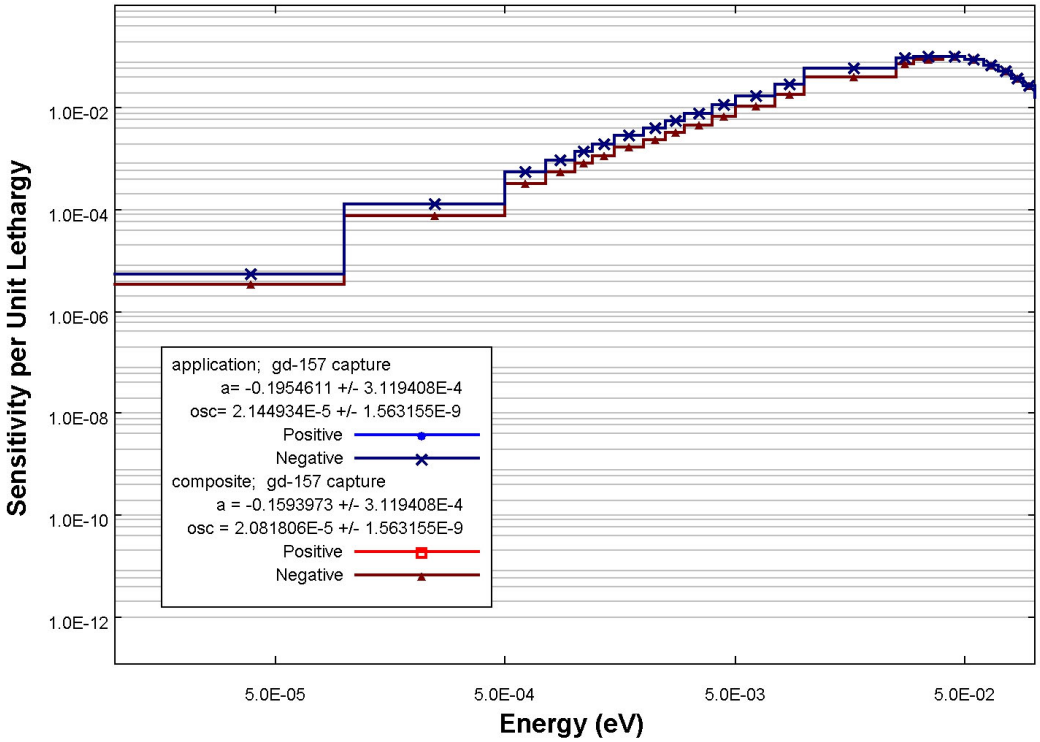

(b) energy range for which $S_a > S_b$

Fig. 12. Composite and application profiles for ^{157}Gd capture.

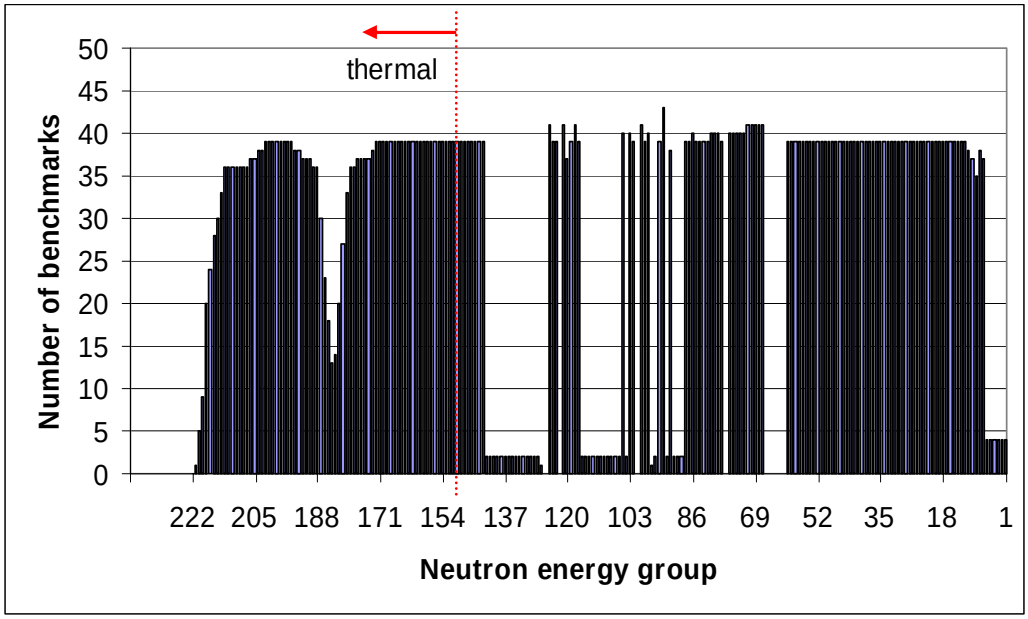

Fig. 13. Number of benchmarks that cover each energy group.

5. EXTENSION OF RESULTS TO THE REMAINING APPLICATION CONFIGURATIONS

The above analysis methodology was extended to the remainder of the application configurations that were identified earlier in this report. The EALF values for all benchmarks and applications are shown in Fig. 14. The case number locations in the figure (x-axis) are arbitrary and correspond to the values given in Table 1 for the applications and in Table A.1 in the Appendix for the benchmarks. The calculated system parameters for these applications are listed in Table 3. The maximum g values for ^{157}Gd capture and sum over energy group of the minimum ^{157}Gd capture sensitivity differences ($Z_a^{j,x}$) for all applications are plotted in Figs. 15 and 16, respectively. In these figures, the practical problem has not been included. As the Gd concentration increases, the g value decreases due to the larger ^{157}Gd capture cross-section sensitivity resulting from the increase in the Gd concentration in the applications. The composite sensitivity profile of the benchmarks for the practical problem and the sensitivity profile for the practical problem are shown in Fig. 17. Between neutron energies 0.08 and 2.0 eV, there is no coverage, as indicated by the smaller composite sensitivity values. The sum of the minimum ^{157}Gd capture sensitivity differences ($Z_a^{j,x}$) for the practical problem is –0.0652.

The sums of the minimum ^{157}Gd capture sensitivity differences ($Z_a^{j,x}$) for 225-L sphere configurations are plotted along with the relevant k_{eff} values in Fig. 18. As expected, as the Gd concentration increases, the sum of the minimum ^{157}Gd capture sensitivity differences increases and the corresponding k_{eff} decreases. The worst-case (largest noncoverage and smallest g value; highlighted with boldfaced type in Table 3) is the 225-L sphere with a H/^{239}Pu of 1000 and 20.445 g/L Gd, which is the practical problem with a k_{eff} value of 0.2434. For this case, the maximum g value for the ^{157}Gd capture cross section is 0.51 and $Z_a^{j,x}$ is –0.0652, which corresponds to 192 noncovered groups. However, due to the very small k_{eff} value (0.2434), the noncoverage results in a negligible penalty (4.82% $\Delta k_{eff}/k_{eff}$) in k_{eff} . The final adjusted k_{eff} value for the practical problem is 0.2551. The adjusted k_{eff} values for 225-L sphere application configurations are also plotted in Fig. 19. As the figure indicates, the penalty due to noncoverage of ^{157}Gd capture sensitivities increases as the Gd concentration increases.

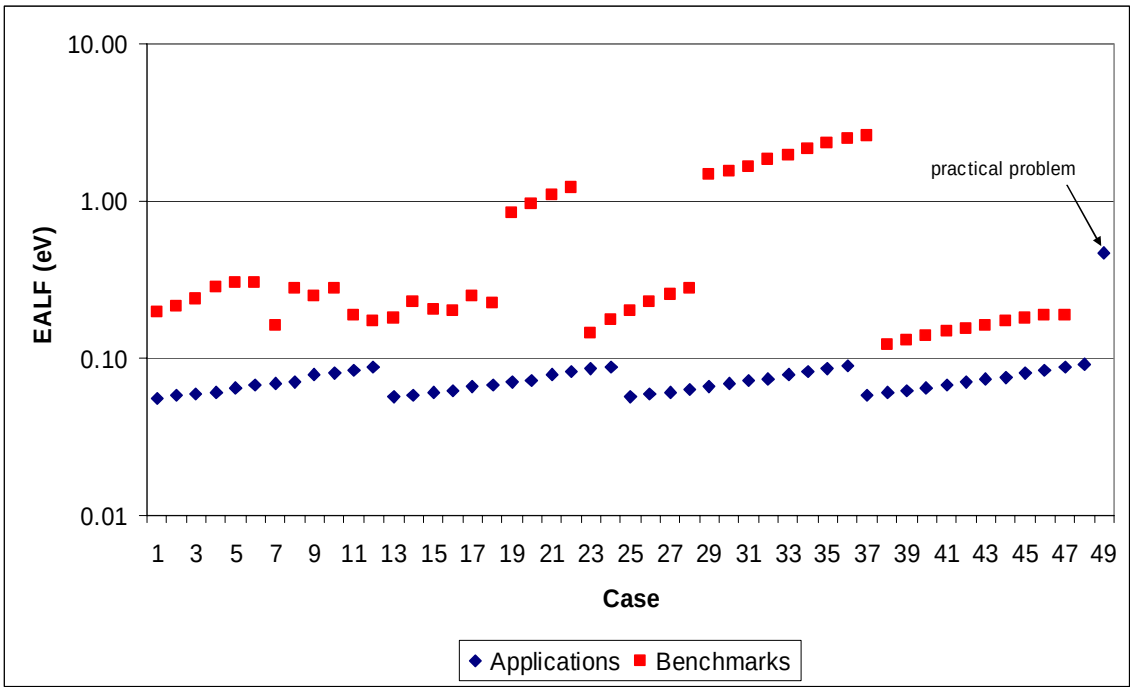

Fig. 14. Energy of average lethargy causing fission (arbitrary case numbers).

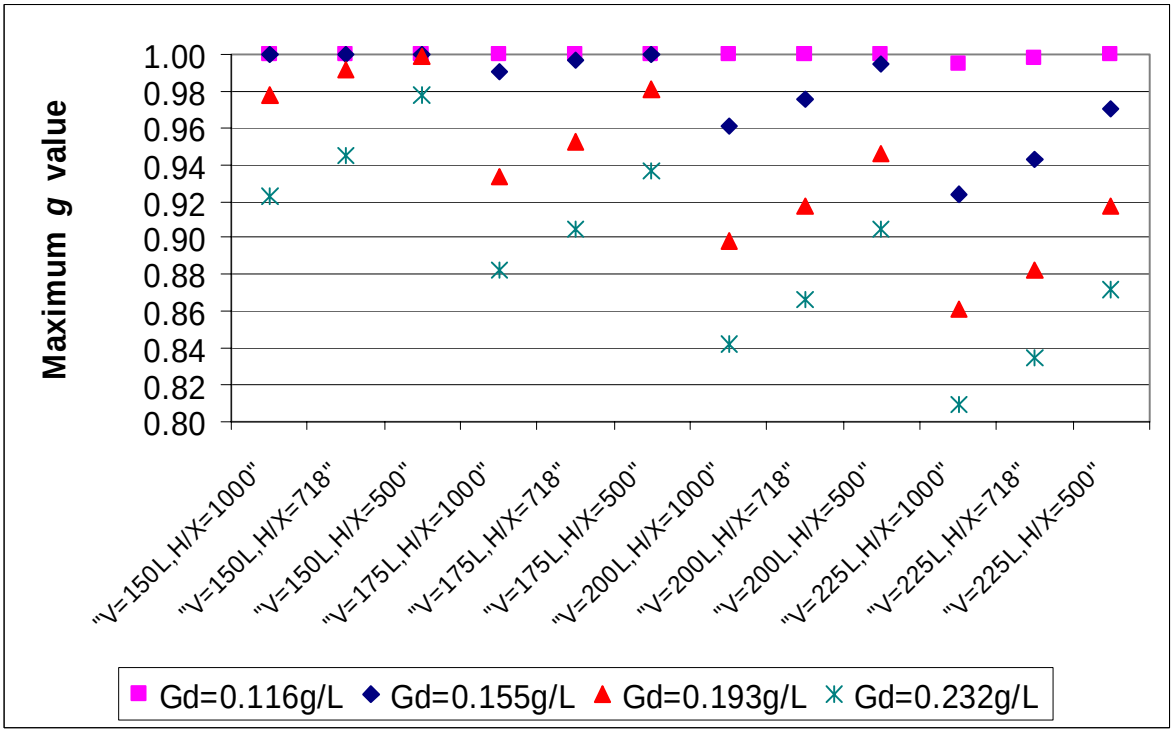

Fig. 15. Maximum *g* value for ^{157}Gd capture for each of 48 applications over all benchmarks.

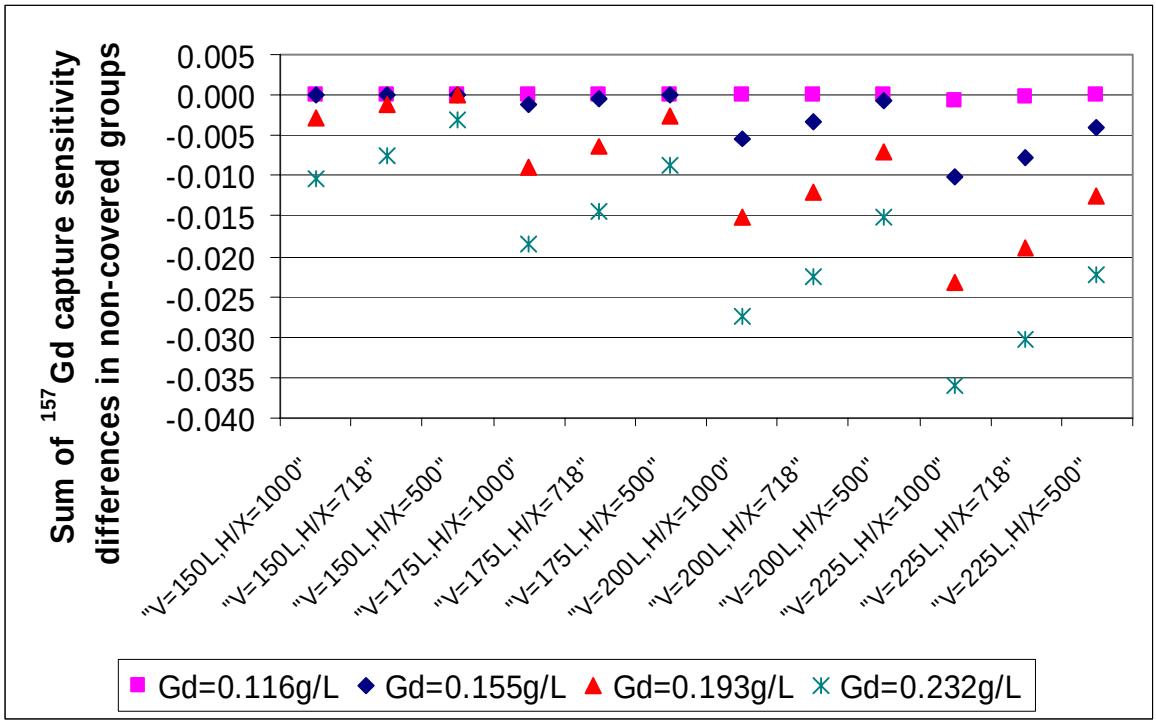

Fig. 16. Sum of the minimum ^{157}Gd sensitivity differences ($Z_a^{j,x}$) for each application.

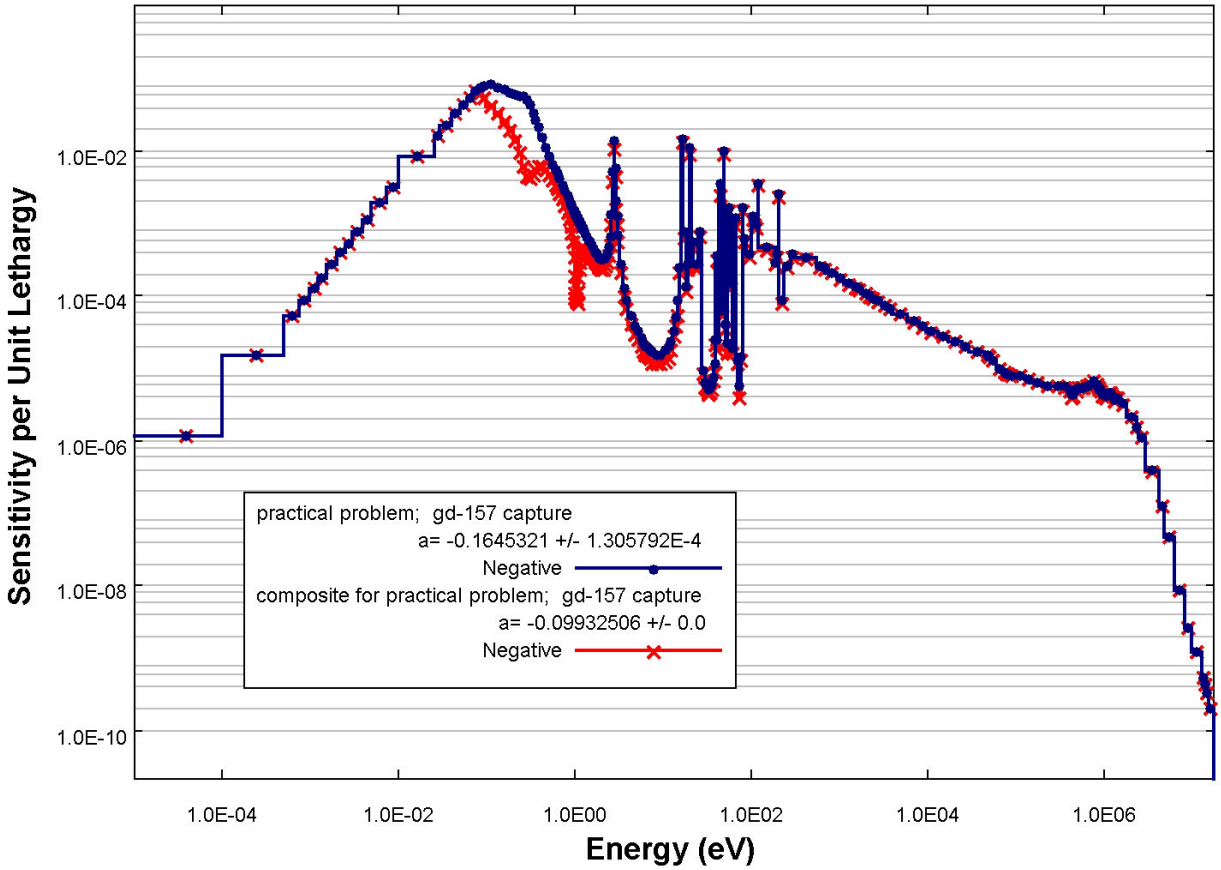

Fig. 17. Profiles of the composite and the practical problem for ^{157}Gd capture.

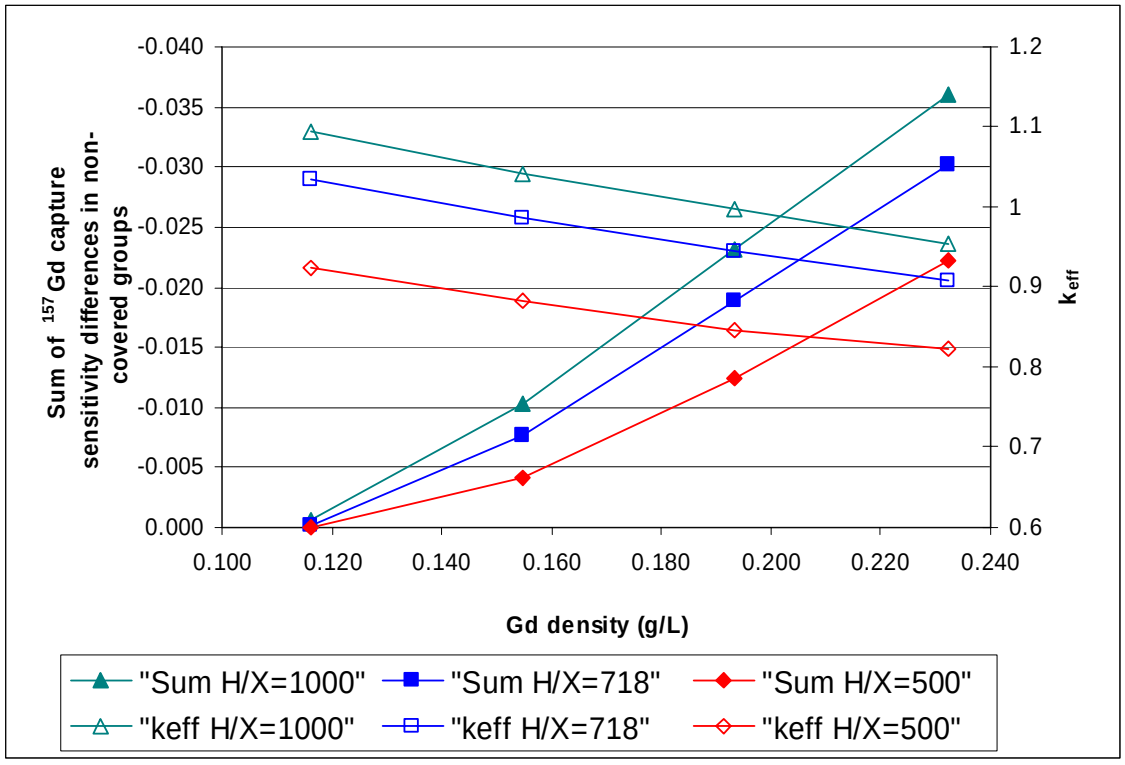

Fig. 18. Sum of the minimum ^{157}Gd sensitivity differences ($Z_a^{j,x}$) and relevant k_{eff} values for 225-L-application configurations.

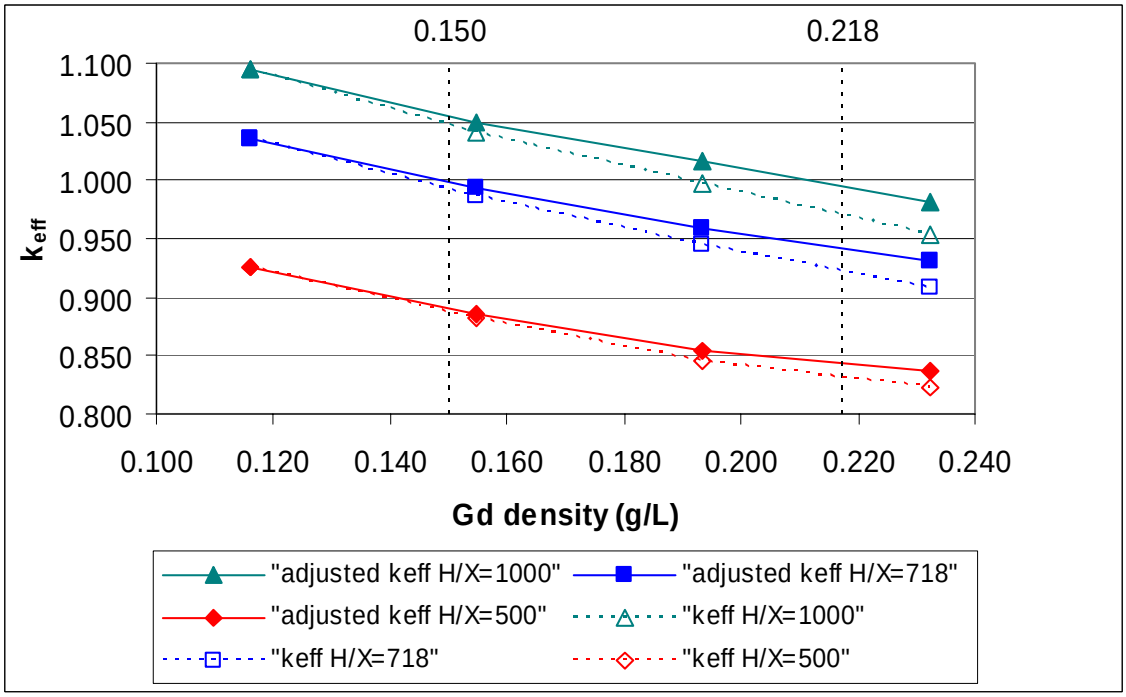

Fig. 19. Calculated and adjusted k_{eff} values for 225-L-application configurations.

Table 3. System characteristics and calculated values for all applications

Sphere volume (L)	H/^{239}Pu	Gd (g/L)	k_{eff}	Maximum g for ^{157}Gd capture	$Z_a^{j,x}$	Penalty ($\%\Delta k_{eff}/k_{eff}$) due to ^{157}Gd capture only	Adjusted k_{eff}	Benchmark that yields largest g for ^{157}Gd capture
150	1000	0.116	1.2314	1.0000	0.0000	0.0000	1.2314	puslgd05
150	1000	0.155	1.1888	0.9998	0.0000	0.0016	1.1888	upuslgd136
150	1000	0.193	1.1485	0.9779	–0.0029	0.2292	1.1511	upuslgd136
150	1000	0.232	1.1147	0.9231	–0.0105	0.8744	1.1244	heust.018-case_12
150	718	0.116	1.2008	1.0000	0.0000	0.0000	1.2008	puslgd04
150	718	0.155	1.1575	1.0000	0.0000	0.0000	1.1575	upuslgd134
150	718	0.193	1.1226	0.9911	–0.0012	0.0972	1.1237	upuslgd136
150	718	0.232	1.0887	0.9452	–0.0074	0.6229	1.0955	upuslgd136
150	500	0.116	1.1027	1.0000	0.0000	0.0000	1.1027	puslgd04
150	500	0.155	1.0693	1.0000	0.0000	0.0000	1.0693	upuslgd133
150	500	0.193	1.0318	0.9994	–0.0001	0.0065	1.0319	upuslgd136
150	500	0.232	1.0048	0.9774	–0.0032	0.2575	1.0074	upuslgd136
175	1000	0.116	1.1749	1.0000	0.0000	0.0000	1.1749	upuslgd133
175	1000	0.155	1.1380	0.9909	–0.0011	0.0954	1.1391	upuslgd136
175	1000	0.193	1.0936	0.9335	–0.0090	0.7549	1.1019	upuslgd136
175	1000	0.232	1.0554	0.8825	–0.0185	1.5322	1.0716	heust.018-case_12
175	718	0.116	1.1381	1.0000	0.0000	0.0000	1.1381	upuslgd133
175	718	0.155	1.0956	0.9966	–0.0004	0.0360	1.0960	upuslgd136
175	718	0.193	1.0555	0.9526	–0.0064	0.5363	1.0612	upuslgd136
175	718	0.232	1.0228	0.9052	–0.0144	1.1972	1.0350	heust.018-case_12
175	500	0.116	1.0373	1.0000	0.0000	0.0000	1.0373	puslgd05
175	500	0.155	1.0004	1.0000	0.0000	0.0000	1.0004	upuslgd135
175	500	0.193	0.9626	0.9811	–0.0026	0.2082	0.9646	upuslgd136
175	500	0.232	0.9348	0.9365	–0.0088	0.7379	0.9417	heust.018-case_12
200	1000	0.116	1.1333	0.9998	0.0000	0.0019	1.1333	upuslgd136
200	1000	0.155	1.0869	0.9610	–0.0053	0.4371	1.0917	upuslgd136
200	1000	0.193	1.0450	0.8985	–0.0152	1.2650	1.0582	heust.018-case_12
200	1000	0.232	1.0045	0.8425	–0.0275	2.2375	1.0270	heust.018-case_12
200	718	0.116	1.0854	1.0000	0.0000	0.0000	1.0854	upuslgd135
200	718	0.155	1.0380	0.9761	–0.0032	0.2580	1.0407	upuslgd136
200	718	0.193	0.9962	0.9170	–0.0119	0.9979	1.0061	heust.018-case_12
200	718	0.232	0.9620	0.8670	–0.0225	1.8356	0.9797	heust.018-case_12
200	500	0.116	0.9810	1.0000	0.0000	0.0000	0.9810	upuslgd133
200	500	0.155	0.9359	0.9950	–0.0007	0.0550	0.9364	upuslgd136
200	500	0.193	0.9064	0.9456	–0.0071	0.6023	0.9119	heust.018-case_12
200	500	0.232	0.8701	0.9049	–0.0150	1.2426	0.8809	heust.018-case_12
225	1000	0.116	1.0948	0.9943	–0.0007	0.0575	1.0954	upuslgd136
225	1000	0.155	1.0412	0.9242	–0.0102	0.8559	1.0501	heust.018-case_12
225	1000	0.193	0.9971	0.8611	–0.0231	1.8928	1.0160	heust.018-case_12
225	**1000**	**0.232**	**0.9537**	**0.8093**	**–0.0361**	**2.9066**	**0.9814**	**heust.018-case_12**
225	718	0.116	1.0356	0.9981	–0.0002	0.0192	1.0358	upuslgd136

Table 3 (continued)

Sphere volume (L)	H/^{239}Pu	Gd (g/L)	k_{eff}	Maximum g for ^{157}Gd capture	$Z_a^{j,x}$	Penalty ($\%\Delta k_{eff}/k_{eff}$) due to ^{157}Gd capture only	Adjusted k_{eff}	Benchmark that yields largest g for ^{157}Gd capture
225	718	0.155	0.9872	0.9431	–0.0077	0.6460	0.9936	upuslgd136
225	718	0.193	0.9439	0.8829	–0.0189	1.5573	0.9586	heust.018-case_12
225	718	0.232	0.9081	0.8354	–0.0302	2.4428	0.9303	heust.018-case_12
225	500	0.116	0.9250	0.9999	0.0000	0.0000	0.9250	upuslgd135
225	500	0.155	0.8825	0.9704	–0.0041	0.3356	0.8855	upuslgd136
225	500	0.193	0.8451	0.9172	–0.0125	1.0424	0.8539	heust.018-case_12
225	500	0.232	0.8221	0.8718	–0.0222	1.8102	0.8370	heust.018-case_12
225	**1000**	**20.445**	**0.2434**	**0.5095**	**–0.0652**	**4.8180**	**0.2551**	**heust.018-case_12**

6. CONCLUSIONS

This reported study demonstrates that there exist some applications for which the Gd (specifically ^{157}Gd capture) cross sections are poorly characterized by the benchmark experiments available for this study. Some of those applications have large k_{eff} values and large sensitivities in noncovered energy groups. Adding much more Gd than is analyzed in this study could make up for the noncoverage since the final k_{eff} would be calculated to be well below 0.82 (the minimum k_{eff} calculated in this study for the range of applications considered) as is the case with the practical problem (i.e., 0.2434). That approach only provides a means to compensate for the inadequacy and ignorance of the Gd cross sections in systems similar to some of the applications considered in this study.

It is concluded that the noncoverage value can be added to the calculated k_{eff} value as a penalty or as an additional term in determining the subcritical margin. The availability of Gd covariance data (or, in general, the covariance data for the nuclide of interest) could lower this penalty value as the cross sections for well-characterized nuclides are generally known with an uncertainty less than 20%, as opposed to the 100% that is assumed for the penalty calculation in this study.

It is evident from this study that to reduce the penalty for Gd cross-section ignorance, as it applies to the assumed applications, more benchmark experiments need to be identified and evaluated, or designed and performed, in order to provide good coverage for systems that are similar to the application systems that were analyzed in this study.

Finally, in determining the coverage and thereby the penalty (if any), as many similar (to the application) benchmarks as possible should be included in the validation benchmark set. The method that has been described in Sect. 3 will take advantage of the similar benchmarks to the extent that the noncoverage will be small. If some benchmarks that are very similar to the application are omitted or are not available in the benchmark set, then the method will yield a higher penalty to reflect that effect. The final penalty value will still depend on the sensitivity to the nuclide-reaction pair of interest and on the uncertainty associated with that pair.

7. REFERENCES

1. B. T. Rearden, "Perturbation Theory Eigenvalue Sensitivity Analysis with Monte Carlo Techniques," *Nucl. Sci. Eng.* (accepted for publication).

2. B. L. Broadhead, B. T. Rearden, C. M. Hopper, J. J. Wagschal, and C. V. Parks, "Sensitivity- and Uncertainty-Based Criticality Safety Validation Techniques," *Nucl. Sci. Eng.* (accepted for publication).

3. S. Goluoglu, C. M. Hopper, and B. T. Rearden, "Extended Interpretation of Sensitivity Data for Benchmark Areas of Applicability," in *Proc. of ANS 2003 Annual Meeting, The Nuclear Technology Expansion: Unlimited Opportunities*, June l–5, 2003, San Diego, Calif. *Trans. Am. Nucl. Soc*. **88**, 77 (2003).

4. *International Handbook of Evaluated Criticality Safety Benchmark Experiments*, NEA/NSC/DOC(95)03, Nuclear Energy Agency Nuclear Science Committee of the Organization for Economic Cooperation and Development (2002).

APPENDIX A

BENCHMARK EXPERIMENTS USED IN THE ANALYSIS

APPENDIX A

BENCHMARK EXPERIMENTS USED IN THE ANALYSIS

Table A.1. List of benchmarks used in the analysis

Case number	Abbreviated name	Input file source	Description
1	e115	ORNL	UO_2 + PuO_2 solids in uranium-plutonium nitrate solution with Gd
2	e116	ORNL	UO_2 + PuO_2 solids in uranium-plutonium nitrate solution with Gd
3	e117	ORNL	UO_2 + PuO_2 solids in uranium-plutonium nitrate solution with Gd
4	e119	ORNL	UO_2 + PuO_2 solids in uranium-plutonium nitrate solution with Gd
5	e120	ORNL	UO_2 + PuO_2 solids in uranium-plutonium nitrate solution with Gd
6	e122	ORNL	UO_2 + PuO_2 solids in uranium-plutonium nitrate solution with Gd
7	heust.018-case_1	IHECSBE	Uranyl nitrate solution
8	heust.018-case_2	IHECSBE	Uranyl nitrate solution
9	heust.018-case_3	IHECSBE	Uranyl nitrate solution
10	heust.018-case_4	IHECSBE	Uranyl nitrate solution with Gd
11	heust.018-case_5	IHECSBE	Uranyl nitrate solution with Gd
12	heust.018-case_6	IHECSBE	Uranyl nitrate solution with Gd
13	heust.018-case_7	IHECSBE	Uranyl nitrate solution with Gd
14	heust.018-case_8	IHECSBE	Uranyl nitrate solution with Gd
15	heust.018-case_9	IHECSBE	Uranyl nitrate solution with Gd
16	heust.018-case_10	IHECSBE	Uranyl nitrate solution with Gd
17	heust.018-case_11	IHECSBE	Uranyl nitrate solution with Gd
18	heust.018-case_12	IHECSBE	Uranyl nitrate solution with Gd
19	mmct112	IHECSBE	MOX fuel pins in uranium-plutonium nitrate solution
20	mmct113	IHECSBE	MOX fuel pins in uranium-plutonium nitrate solution
21	mmct114	IHECSBE	MOX fuel pins in uranium-plutonium nitrate solution
22	mmct116	IHECSBE	MOX fuel pins in uranium-plutonium nitrate solution
23	puslgd01	SRS	$Pu(NO_3)_4$ solution with Gd
24	puslgd02	SRS	$Pu(NO_3)_4$ solution with Gd
25	puslgd03	SRS	$Pu(NO_3)_4$ solution with Gd
26	puslgd04	SRS	$Pu(NO_3)_4$ solution with Gd
27	puslgd05	SRS	$Pu(NO_3)_4$ solution with Gd
28	puslgd06	SRS	$Pu(NO_3)_4$ solution with Gd
29	puslgd07	SRS	$Pu(NO_3)_4$ solution with Gd
30	puslgd08	SRS	$Pu(NO_3)_4$ solution with Gd
31	puslgd09	SRS	$Pu(NO_3)_4$ solution with Gd
32	puslgd10	SRS	$Pu(NO_3)_4$ solution with Gd
33	puslgd11	SRS	$Pu(NO_3)_4$ solution with Gd
34	puslgd12	SRS	$Pu(NO_3)_4$ solution with Gd
35	puslgd13	SRS	$Pu(NO_3)_4$ solution with Gd

Table A.1 (continued)

Case number	Abbreviated name	Input file source	Description
36	puslgd14	SRS	$Pu(NO_3)_4$ solution with Gd
37	puslgd15	SRS	$Pu(NO_3)_4$ solution with Gd
38	upuslgd127	ORNL	$UO_2(NO_3)_2 + Pu(NO_3)_4$ solution with Gd
39	upuslgd128	ORNL	$UO_2(NO_3)_2 + Pu(NO_3)_4$ solution with Gd
40	upuslgd129	ORNL	$UO_2(NO_3)_2 + Pu(NO_3)_4$ solution with Gd
41	upuslgd130	ORNL	$UO_2(NO_3)_2 + Pu(NO_3)_4$ solution with Gd
42	upuslgd131	ORNL	$UO_2(NO_3)_2 + Pu(NO_3)_4$ solution with Gd
43	upuslgd132	ORNL	$UO_2(NO_3)_2 + Pu(NO_3)_4$ solution with Gd
44	upuslgd133	ORNL	$UO_2(NO_3)_2 + Pu(NO_3)_4$ solution with Gd
45	upuslgd134	ORNL	$UO_2(NO_3)_2 + Pu(NO_3)_4$ solution with Gd
46	upuslgd135	ORNL	$UO_2(NO_3)_2 + Pu(NO_3)_4$ solution with Gd
47	upuslgd136	ORNL	$UO_2(NO_3)_2 + Pu(NO_3)_4$ solution with Gd

Table A.2. Concentrations of Gd in benchmark experiments

Benchmark abbreviated name	Gd concentration (g/L)	Benchmark abbreviated name	Gd concentration (g/L)
e115	0.02	puslgd01	0
e116	0.258	puslgd02	0.48
e117	0.515	puslgd03	0.96
e119	1.04	puslgd04	1.42
e120	1.28	puslgd05	1.92
e122	1.338	puslgd06	2.38
heust.018-case_1	0	puslgd07	4.4
heust.018-case_2	0	puslgd08	5.28
heust.018-case_3	0	puslgd09	6.28
heust.018-case_4	0.497	puslgd10	8.21
heust.018-case_5	0.497	puslgd11	9.88
heust.018-case_6	0.497	puslgd12	12.58
heust.018-case_7	0.977	puslgd13	15.55
heust.018-case_8	0.977	puslgd14	18.4
heust.018-case_9	0.977	puslgd15	20.25
heust.018-case_10	1.4	upuslgd127	0.042
heust.018-case_11	1.4	upuslgd128	0.18
heust.018-case_12	1.943	upuslgd129	0.288
mmct112	0.49	upuslgd130	0.459
mmct113	0.98	upuslgd131	0.581
mmct114	1.47	upuslgd132	0.679
mmct116	2.16	upuslgd133	0.8
		upuslgd134	0.923
		upuslgd135	1.01
		upuslgd136	1.06

INTERNAL DISTRIBUTION

1. B. L. Broadhead, 5700, MS-6170
2. W. C. Carter, 5700, MS-6170
3. M. D. DeHart, 5700, MS-6170
4. M. E. Dunn, 5700, MS-6170
5. K. R. Elam, 5700, MS-6170
6. I. C. Gauld, 5700, MS-6170
7. L. L. Gilpin, 2518, MS-6301
8. S. Goluoglu, 5700, MS-6170
9. J. N. Herndon, 4500N, MS-6248
10. D. J. Hill, 5700, MS-6152
11. D. F. Hollenbach, 5700, MS-6170
12. C. M. Hopper, 5700, MS-6170
13. L. C. Leal, 5700, MS-6170
14. D. Mueller, 4500S, MS-6127
15. C. V. Parks, 5700, MS-6170
16. L. M. Petrie, 5700, MS-6170
17. R. T. Primm, III, 7917, MS-6399
18. B. T. Rearden, 5700, MS-6170
19. D. A. Reed, 4500S, MS-6127
20. J. C. Wagner, 5700, MS-6170
21. R. M. Westfall, 5700, MS-6170
22. M. L. Williams, 5700, MS-6170
23. ORNL OTIC–RC, 6011, MS-6283

EXTERNAL DISTRIBUTION

24. R. E. Anderson, HSR-6, MS F691, Los Alamos National Laboratory, Los Alamos, NM 87545
25. J. B. Briggs, Idaho National Engineering and Environmental Laboratory, Radiation Physics, PO Box 1625, Mail Stop 3855, Idaho Falls, ID 83415
26. D. E. Carlson, U.S. Nuclear Regulatory Commission, RES/DSARE/REAHFB, MS T10 F13A, Washington, DC 20555-0001
27. K. J. Carroll, BWXT Y-12, Y-12 National Security Complex, PO Box 2009, MS 8238, Oak Ridge, TN 37831-8238
28. M. S. Chatterton, U.S. Nuclear Regulatory Commission, NMSS/FCSS/SPIB, MS T8 A33, Washington, DC 20555-0001
29. D. H. Crandall, NA-11/Forrestal Building, U.S. Department of Energy, 1000 Independence Ave., Washington, DC 20585
30. M. Dayani, Office of the Manager, Y-12, Bldg. 9704-2, Rm. 186A, MS-8009, Oak Ridge, TN 37831
31. J. P. Drago, CH/Building 201, U.S. Department of Energy, Chicago Operations Office, 9800 S. Cass Avenue, Argonne IL 60439
32. H. D. Felsher, U.S. Nuclear Regulatory Commission, NMSS/FCSS/SPIB, MS T8 A33, Washington, DC 20555-0001
33. J. R. Felty, Science Applications Intl. Corp., 2418 N. Dickerson St., Arlington, VA 22207
34. I. E. Fergus, QA-50/Germantown Building GTN, U.S. Department of Energy, 1000 Independence Ave., SW, Washington, DC 20585-1290
35. Adolf Garcia, Idaho National Engineering and Environmental Laboratory, 2525 North Fremont Avenue, Idaho Falls, ID 83401
36. K. Grooms, U.S. Department of Energy, Argonne Group, 9800 South Cass Avenue, Argonne, IL 60439
37. B. Hawks, U.S. Department of Energy, Oak Ridge Operations Office, 200 Administration Road, Oak Ridge, TN 37831
38. Song Huang, Lawrence Livermore National Laboratory, 7000 East Avenue, MS L-128, Livermore, CA 94550
39. S. L. Johnson, EM-5/Forrestal Building, U.S. Department of Energy, 1000 Independence Ave., Washington, DC 20585
40. Ed Kendall, BWXT Y-12, PO Box 2009, Bldg. 9704-2, MS-8007, Oak Ridge, TN 37831-8007

41. K. D. Kimball, NISYS Corporation, 4233 Pleasant Hill Rd (Suite 200), Duluth, GA 30096
42. Ron Knief, 10036 Wellington NE, Albuquerque, NM 87111
43. Mark Lee, University of California, Lawrence Livermore National Laboratory, 7000 East Avenue, PO Box 808, L-1, Livermore, CA 94550
44. C. D. Manning, Framatome Advanced Nuclear Power, 2101 Horn Rapids Road, Richland, WA 99352-5102
45. Robert McBroom, U.S. Department of Energy, Oak Ridge Operations Office, 200 Administration Road, Oak Ridge, TN 37831
46. Jerry McKamy, EH-21/Germantown Building 270CC, U.S. Department of Energy, 1000 Independence Ave., SW, Washington, DC 20585-1290
47. T. P. McLaughlin, Los Alamos National Laboratory, Bikini Atoll Rd., SM 30, PO Box 1663 (MS F691), Los Alamos, NM 87545
48. Richard D. McKnight, Nuclear Engineering Division - Bldg. 208, Argonne National Laboratory, 9700 S. Cass Avenue, Argonne, IL 60439
49. Dr. James A. Morman, Argonne National Laboratory, 9700 S. Cass Ave., Bldg 208, Argonne, IL 60439
50. D. M. Neil, Department of Energy, 800 DOE Drive, MS-4160, Idaho Falls, ID 83401
51. Bob Nelson, U.S. Department of Energy, Richland Operations Office, 825 Jadwin Avenue, PO Box 550, Richland, WA 99352
52. T. Nirider, U.S. Department of Energy, Richland Operations Office, 825 Jadwin Avenue, PO Box 550, Richland, WA 99352
53. N. L. Osgood, U.S. Nuclear Regulatory Commission, NMSS/SFPO/SFLS, MS O13 D13, Washington, DC 20555-0001
54. L. E. Paulson, M/C K-26, Global Nuclear Fuel, 3901 Castle Hayne Road, Wilmington, NC 28402
55. Steve Payne, U.S. Department of Energy Albuquerque Operations Office, Pennsylvania & H Street, Kirtland Air Force Base, Albuquerque, NM 87116
56. Chad Pope, Argonne West National Laboratory, PO Box 2528, Idaho Falls, ID 83403
57. Andrew Prichard, Battelle, Pacific Northwest National Lab, PO Box 999 / MS K8-34, Richland, WA 99352
58. M. Brady-Raap, Pacific Northwest Laboratory, PO Box 999, MS K8-34, Richland, WA 99352
59. B. Reed, Battelle, Pacific Northwest National Lab, PO Box 999 / MS K8-34, Richland, WA 99352
60. T. Reilly, Westinghouse Savannah River Co., PO Box 616, Routing WSMS, Aiken, SC 29808
61. Kevin Reynolds, U.S. Department of Energy, Oak Ridge Operations Office, 200 Administration Road, Oak Ridge, TN 37831
62. R. C. Robinson, BWXT Y-12, PO Box 2009, Bldg. 9110, MS-8238, Oak Ridge, TN 37831-8238
63. Frank Schwartz, 1 Mound Road, Box 66, Miamisburg, OH 45343
64. Don Scott, Westinghouse Savannah River Co., PO Box 616, Aiken, SC 29808
65. Shiv Seth, U.S. Department of Energy, Richland Operations Office, 825 Jadwin Avenue, PO Box 550, Richland, WA 99352
66. Norm Shepard, Westinghouse Savannah River Co., PO Box 616, Aiken, SC 29808
67. J. T. Taylor, Bechtel BWXT - Idaho, PO Box 1625, MS 3458, Idaho Falls, ID 83415
68. M. A. Thompson, NA-117/Germantown Building GTN, U.S. Department of Energy, 1000 Independence Ave., SW, Washington, DC 20585-1290
69. Hans Toffer, U.S. Department of Energy, Richland Operations Office, 825 Jadwin Avenue, PO Box 550, Richland, WA 99352

70–75. E. Fitz Trumble, Westinghouse Safety Management Solutions, PO Box 5388, 1993 South Centennial Dr., Aiken, SC 29803

76. J. J. Wagschal, Racah Institute of Physics, The Hebrew University of Jerusalem, 91904, Jerusalem, ISRAEL
77. D. W. Williams, Westinghouse NFD – MS 15, 5801 Bluff Road, Columbia, SC 29209

78. Bruce A Wilson, Bechtel Jacobs, LLC, Building 1320, MS-7583, P.O. Box 4699,Oak Ridge, TN 37831-7583
79. R. E. Wilson, U.S. Department of Energy, Rocky Flats Field Office, 10808 Highway 93, Unit A, Golden, CO 80403-8200
80. C. J. Withee, U.S. Nuclear Regulatory Commission, NMSS/SFPO/TRB, MS O13 D13, Washington, DC 20555-0001
81. C. A. Worley, BWXT Y-12, PO Box 2009, Bldg. 9110, MS-8238, Oak Ridge, TN 37831-8238